



# Particles in the great Pinatubo volcanic cloud of June 1991: The role of ice

**Song Guo**

*Department of Geological Engineering and Sciences, Michigan Technological University, Houghton, Michigan 49931, USA*

*Now at Department of Atmospheric and Oceanic Sciences, McGill University, 805 Sherbrooke Street West, Montreal, Quebec, Canada H3A 2K6 (songguo@zephyr.meteo.mcgill.ca)*

**William I. Rose, Gregg J. S. Bluth, and I. Matthew Watson**

*Department of Geological Engineering and Sciences, Michigan Technological University, Houghton, Michigan 49931, USA*

[1] Pinatubo's 15 June 1991 eruption was Earth's largest of the last 25 years, and it formed a substantial volcanic cloud. We present results of analysis of satellite-based infrared remote sensing using Advanced Very High Resolution Radiometer (AVHRR) and TIROS Operational Vertical Sounder/High Resolution Infrared Radiation Sounder/2 (TOVS/HIRS/2) sensors, during the first few days of atmospheric residence of the Pinatubo volcanic cloud, as it drifted from the Philippines toward Africa. An SO<sub>2</sub>-rich upper (25 km) portion drifted westward slightly faster than an ash-rich lower (22 km) part, though uncertainty exists due to difficulty in precisely locating the ash cloud. The Pinatubo clouds contained particles of ice, ash, and sulfate which could be sensed with infrared satellite data. Multispectral IR data from HIRS/2 were most useful for sensing the Pinatubo clouds because substantial amounts of both ice and ash were present. Ice and ash particles had peak masses of about 80 and 50 Mt, respectively, within the first day of atmospheric residence and declined very rapidly to values that were <10 Mt within 3 days. Ice and ash declined at a similar rate, and it seems likely that ice and ash formed mixed aggregates which enhanced fallout. Sulfate particles were detected in the volcanic cloud by IR satellites very soon after eruption, and their masses increased systematically at a rate consistent with their formation from SO<sub>2</sub>, which was slowly decreasing in mass during the same period. The initially detected sulfate mass was 4 Mt (equivalent to 3 Mt SO<sub>2</sub>) and after 5 days was 12–16 Mt (equivalent to 9–12 Mt SO<sub>2</sub>).

**Components:** 12,820 words, 29 figures, 9 tables, 2 animations.

**Keywords:** ash, ice, and sulfate particles; Pinatubo Volcanic Cloud; satellite remote sensing.

**Index Terms:** 0370 Atmospheric Composition and Structure: Volcanic effects (8409); 0305 Atmospheric Composition and Structure: Aerosols and particles (0345, 4801); 1640 Global Change: Remote sensing.

**Received** 25 October 2003; **Revised** 2 March 2004; **Accepted** 22 March 2004; **Published** 8 May 2004.

Guo, S., W. I. Rose, G. J. S. Bluth, and I. M. Watson (2004), Particles in the great Pinatubo volcanic cloud of June 1991: The role of ice, *Geochem. Geophys. Geosyst.*, 5, Q05003, doi:10.1029/2003GC000655.

## 1. Introduction

[2] Mount Pinatubo is located at 15°08'N, 120°21'E in western Luzon, Philippines. After

weeks of precursory volcanic activity, a climactic eruption occurred around 13:42 (local time) on 15 June 1991 and lasted for approximately 9 hours [Wolfe and Hoblitt, 1996]. It is the largest eruption

**Table 1.** Characteristics of TOMS, HIRS/2, and AVHRR Satellite Sensors Used in This Paper

TOMS <sup>a</sup>			AVHRR <sup>b</sup>			HIRS/2 <sup>b</sup>		
Spatial Resolution: 50 km (nadir)			Spatial Resolution: 4.4 km (GAC)			Spatial Resolution: 17.5 km (nadir)		
Channel	Wavelength, nm	Usage	Channel	Wavelength, $\mu\text{m}$	Usage	Channel	Wavelength, $\mu\text{m}$	Usage
1	308.6	SO <sub>2</sub>	4	10.3–11.3	Ash, ice	5	13.97	ash, ice, sulfate
2	313.5	SO <sub>2</sub>	5	11.5–12.5	Ash, ice	6	13.64	ash, ice, sulfate
3	317.5	SO <sub>2</sub>				7	13.35	ash, ice, sulfate
4	322.3	SO <sub>2</sub>				8	11.11	ash, ice, sulfate
5	331.2	SO <sub>2</sub> , AI				9	9.71	ash, ice, sulfate
6	360.48	AI				10	8.16	ash, ice, sulfate
						11	7.33	SO <sub>2</sub> <sup>c</sup>

<sup>a</sup>McPeters *et al.* [1998].

<sup>b</sup>Yu and Rose [2000].

<sup>c</sup>Prata *et al.* [2003].

of the past 25 years based on its eruption volume (8.4–10.4 km<sup>3</sup> total ejecta bulk volume estimated by Scott *et al.* [1996]) and its aerosol perturbation to the stratosphere [McCormick *et al.*, 1995]. Huge masses of volcanic ash and gas, or mixtures of them with hydrometeors, were directly emitted into stratosphere and produced significant global environmental, atmospheric, and climatic effects for up to several years [McCormick *et al.*, 1995; Self *et al.*, 1996; Robock, 2002]. The most significant atmospheric effects include the following: (1) The large stratospheric sulfate aerosol loading with chemical and dynamic perturbations affecting the stratospheric NO<sub>2</sub>, reactive chlorine, and ozone concentrations and increasing the stratospheric opacity [McCormick *et al.*, 1995]. (2) The effects on the global radiative processes

causing the coexistence of cooling effects in the troposphere (more solar radiation scattering back to space) and warming effects in the stratosphere (infrared absorptivity of stratospheric aerosols) [McCormick *et al.*, 1995]. Summer surface cooling and winter surface warming were found in the northern hemisphere 1–2 years after eruption [Robock, 2002]. (3) The destruction of stratospheric ozone occurring due to both heterogeneous reactions occurring on the surface of sulfate aerosol (similar to heterogeneous reactions that occur within polar stratospheric clouds responsible for the Antarctic Ozone Hole [Solomon *et al.*, 1993]) and circulation changes after the eruption [Kinne *et al.*, 1992]. (4) Climatic effects which lasted for up to several years after eruption [Robock, 2002].

**Table 2.** Data Sets Used in This Study From AVHRR and HIRS/2<sup>a</sup>

Date	NOAA-10	NOAA-11		NOAA-12	
	HIRS/2	AVHRR	HIRS/2	AVHRR	HIRS/2
6/15/91		06:30	06:30	10:20&12:06	
	10:26	17:58&19:41	18:08		10:53
6/16/91	00:52	07:26	07:28	10:00&11:44	01:18
	11:44	20:05	20:05		12:20
6/17/91	00:12–00:33	07:19&09:00	07:25–08:43	11:21&13:01	00:39–02:01
	11:39–13:05	19:16&20:59	19:16–20:59		12:07–13:31
6/18/91	01:55–04:58	05:51&07:25&08:43	07:26–08:43	12:41&14:34&16:08	02:21–05:25
	12:41–16:08	20:47&22:22&23:59	20:47–21:22		12:53–16:05
6/19/91	01:58–03:41	08:38&10:20&12:04	07:25–08:43	12:21&14:05&15:44	02:20–05:25
	12:41–16:08		20:47–21:22		12:53–16:05

<sup>a</sup>Note: All times listed are UTC. The AVHRR and HIRS/2 sensors are on board the same platform. The AVHRR image times are the central pixel sensing time if only one orbit involved or the central pixel sensing times of each individual orbit. The HIRS/2 image time is either the central pixel sensing time if only one orbit involved or the central pixel sensing times of the starting and ending orbits if more than more orbit involved.

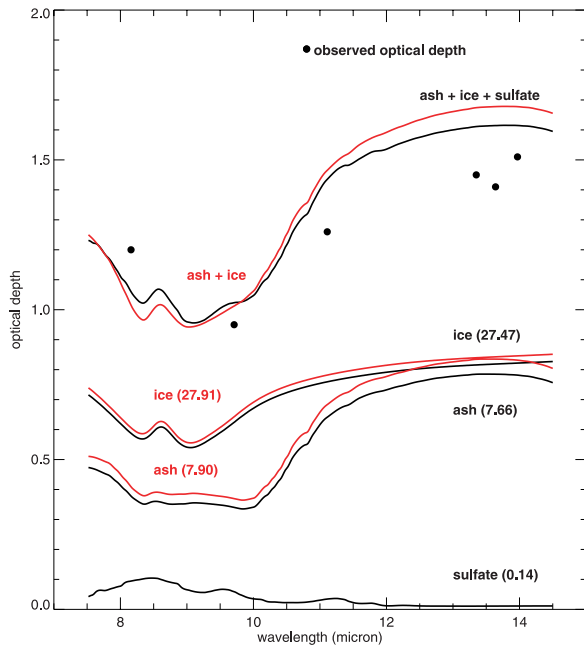


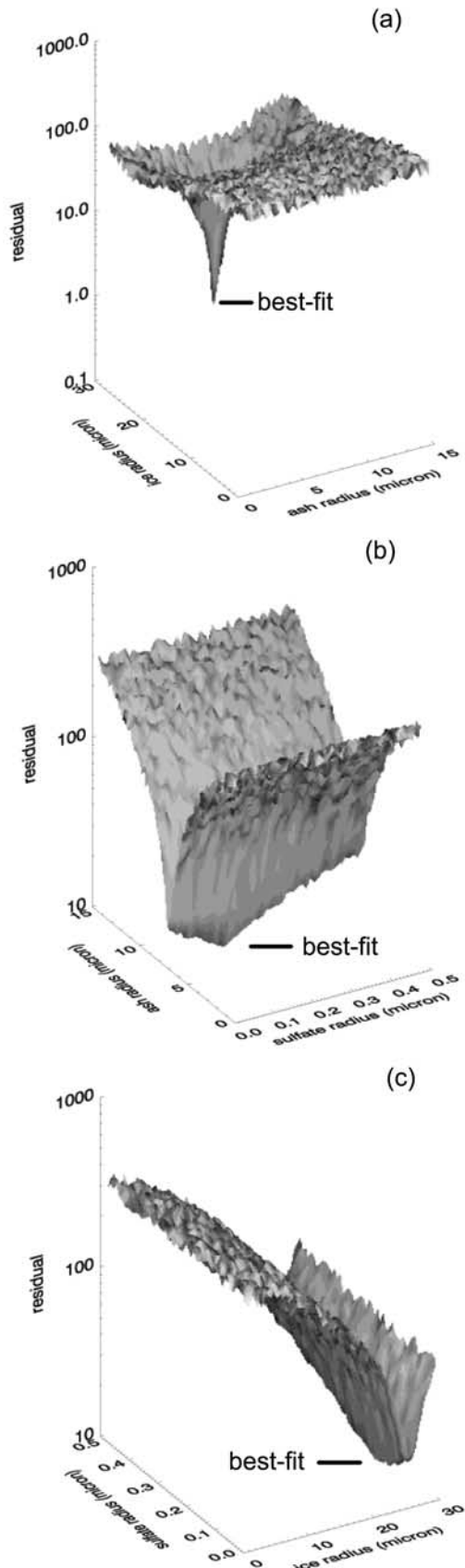
**Figure 1.** Plot to demonstrate the proportional contribution to optical depth of the various kinds of particles in the Pinatubo volcanic cloud based on the modified method of *Yu and Rose* [2000]. Three curves representing the optimum uniform sizes of the three particle types are plotted along with the sums in parentheses. A similar result using only two particle types (ash and ice) is also shown for comparison in red. The points plotted are the average values of optical depth observed in the HIRS/2 volcanic cloud of 11:44 UT (16 June 1991). The residuals of the deviation between the points and the two summed optical depth curves are used to find the best fit. Note that the optimal sizes for ash and ice do not differ much whether the 2 or 3 component match is attempted. Note also the total optical depth for sulfate is small. These observations show that the proportions of ice and ash dominate the signal.

[3] In spite of its significance, Pinatubo has not been studied with volcanic cloud particle retrieval methods. AVHRR data have been used to trace the spatial development of the Pinatubo volcanic clouds and to observe gravity currents [*Long and Stowe, 1994; Holasek et al., 1996; Self et al., 1996*]. Study of sequential AVHRR imagery was challenging because of its scale and tropical location: (1) The Pinatubo clouds are so widespread that multiple orbits must be combined to see the whole volcanic cloud; (2) it is sometimes difficult to distinguish the Pinatubo volcanic clouds from other interferences (e.g., tropical convective clouds, upper tropospheric saharan dust, and

Typhoon Yunya), some of which also have negative BTD (Brightness Temperature Difference of band 4 and 5) values; (3) only the central portions of the volcanic ash clouds can be detected by the split-window method (negative BTD value scheme) as the high water vapor contents below the ash cloud cause the positive shift of the BTD values of the ash dominant pixels [*Yu et al., 2002*]; and (4) during the first ~20 hours after the eruption, parts of the ash cloud remained opaque to infrared sensors owing to its high optical thickness.

[4] The separation of the gas-rich portions and ash-rich portions of volcanic clouds have been observed in most eruptions studied with satellite data [*Bluth et al., 1994; Rose et al., 1995; Schneider et al., 1999; Shannon, 1997; Mayberry et al., 2002; Constantine et al., 2000*] with the notable exception of 1992 Mount Spurr eruption [*Schneider et al., 1995; Rose et al., 2001*]. These separations might be due to the fact that SO<sub>2</sub> rises higher in the plume than the volcanic ash [*Rose et al., 2000*] over the eruption vent; differences of wind directions and speeds at different altitudes will cause horizontal separation.

[5] In this paper, we apply methods for IR retrievals of particles in the Pinatubo cloud for the first several days of its atmospheric residence. Fourteen AVHRR ash maps and twenty-eight HIRS/2 images the first five days after eruption are analyzed to study the particle properties within the Pinatubo volcanic clouds using the AVHRR two-band split-window retrieval [*Wen and Rose, 1994*] and HIRS/2 multiband retrieval [*Yu and Rose, 2000*], respectively. The atmospheric correction method developed by *Yu et al.* [2002] is applied to improve the AVHRR retrievals. The adverse effects on the AVHRR two-band split-window retrieval caused by the contrary effects of ash and ice are studied. Simultaneous retrieval of ash, ice, and sulfate properties using multiband HIRS/2 data for the Pinatubo volcanic clouds allows us to consider how the different particles may interact. The retrieved ash properties and derived ash removal rates are compared with those of the 1982 El Chichón and other smaller eruptions. The movement of Pinatubo's SO<sub>2</sub> and ash clouds are also investigated with the NASA GSFC



isentropical wind trajectory results to estimate the altitudes of the SO<sub>2</sub>-rich and ash-rich clouds.

## 2. Satellite Data

[6] The characteristics of multispectral satellite sensors used in this paper are summarized in Table 1.

[7] The Pinatubo fine ash (1–12 μm) cloud remained visible to the AVHRR sensor for 104 hours after the start of eruption. Fine ash (1–15 μm; reflecting a slightly different size discrimination sensitivity from AVHRR) was detected by HIRS/2 sensor for 111 hours. The 14 AVHRR and 28 HIRS/2 satellite maps used in this paper are summarized in Table 2. The first three days' TOMS SO<sub>2</sub> and TOMS AI (Aerosol Index, see definition below) maps (TOMS AI is only visible for the first ~46 hours after eruption) are also used to supplement the IR retrievals.

## 3. Methodology

### 3.1. Volcanic Ash Detection With TOMS AI

[8] Volcanic ash and other types of aerosols can be qualitatively detected by the TOMS AI (Aerosol Index) method. AI is defined as the difference of the measured spectral contrast between the 331.2 nm and 360.48 nm radiances and the spectral contrast between the 331.2 nm and 360.48 nm radiances calculated for a Rayleigh scattering atmosphere and Lambertian surface [Seftor *et al.*, 1997; Krotkov *et al.*, 1999]. Absorbing aerosols (volcanic ash, smoke, desert dust) usually have

**Figure 2.** Logarithmic plots of the residual from fit for various two-component combinations of particles in the Pinatubo volcanic cloud. A well-defined single residual minimum for ash-ice mixtures is identified in the results (Figure 2a). The plots with sulfate (Figures 2b and 2c) show that the best fit represents a slight minimum point along two trough-like valleys. This suggests that the sulfate sizes and masses are not as well constrained as the ash-ice relations. The actual retrieval we use is three-dimensional, so visualization of ash-ice-sulfate relationships is difficult. Figures 1 and 2 are included to help the reader visualize how the multiband retrieval [Yu and Rose, 2000] works.

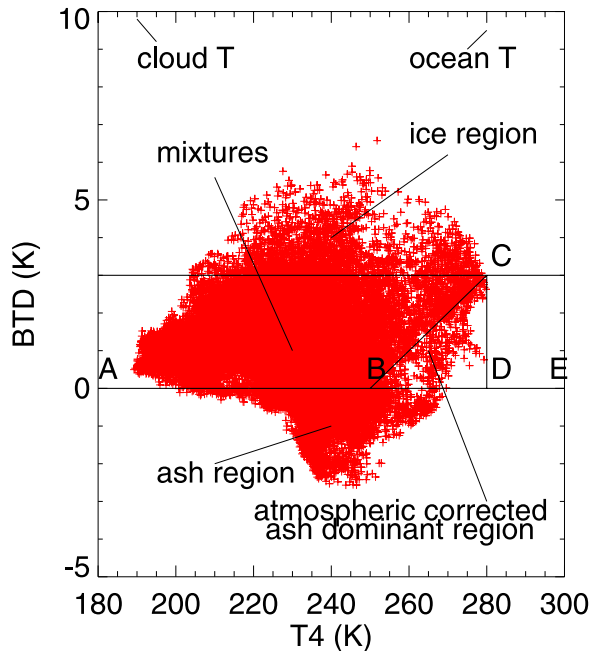


**Figure 3.** Brightness temperature differences of band 4 minus band 5 (BTD) versus band 4 brightness temperature (T4) for pixels from the 16 June 20:05 (GMT) Pinatubo volcanic cloud measured by AVHRR. The negative BTD value region (15.9% of all pixels) represents pixels dominated by ash particles. The upper field (BTD > 3.0) region (4.1% of all pixels) represents an “ice region” where ice is the dominant particle type in the pixel region. The triangular region (1.7% of all pixels) bounded by points B, C, and D represents an atmospheric moisture/vapor correction region which could reflect optically thin, ash-dominant pixels. The region labeled “mixtures” (78.3% of all pixels) represents pixels which appear to be the result of significant masses of both ash and ice, consisting either of both ice and ash or hybrid mixtures (icy ash balls). The atmospherically corrected AVHRR two-band split-window method can detect ash pixels below the line AE (BTD < 0) and within triangular area BCD. The ice signals might be counteracted by ash signals in the AVHRR retrieval. Many large stratospheric volcanic clouds have ash regions which extend to much lower BTD values, as low as  $-15$  to  $-20$ , and the lack of such low values here is another sign of ice.

positive AI values while non-absorbing aerosols (e.g., sulfate aerosol) usually have negative AI values [Seftor *et al.*, 1997].

### 3.2. AVHRR Two-Band Split-Window Retrieval

[9] Two thermal bands (band 4, 10.3 to 11.3  $\mu\text{m}$ , and band 5, 11.5 to 12.5  $\mu\text{m}$ ) of AVHRR have been

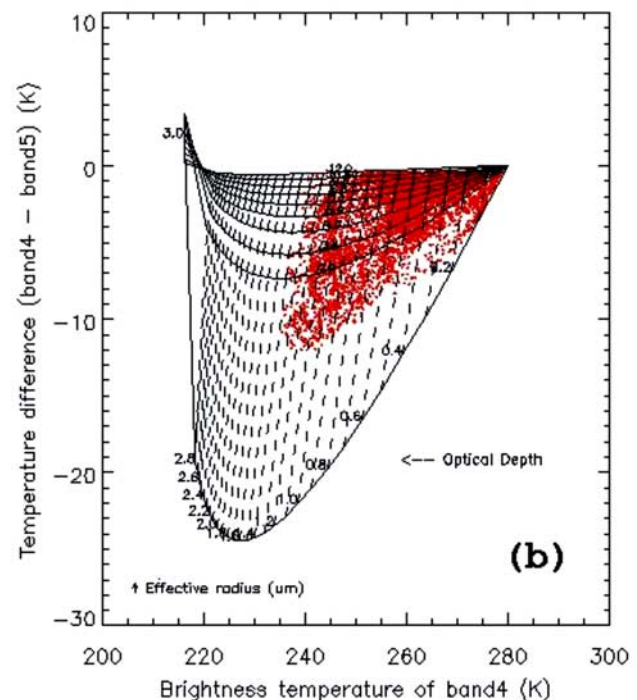
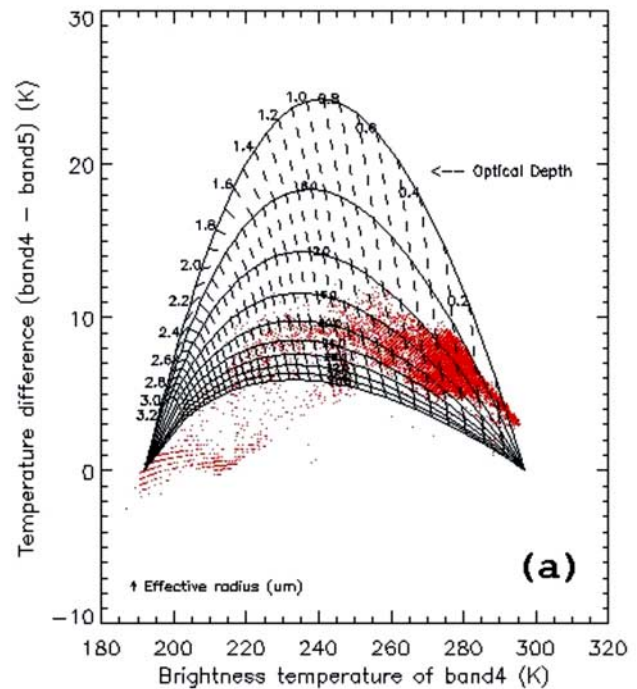


**Figure 4.** Brightness temperature differences (BTD) of band 4 minus band 5 versus band 4 brightness temperature (T4) from NOAA 12 AVHRR ash maps from Rose *et al.* [1995]. (a) Rabaul eruption at 09:00 (GMT) on 19 September 1994, showing ice particles within the volcanic cloud which have positive BTD values. (b) Klyuchevskoi eruption at 06:40 (GMT) on 1 October 1994, showing typical ash dominant volcanic clouds, which have negative BTD values.

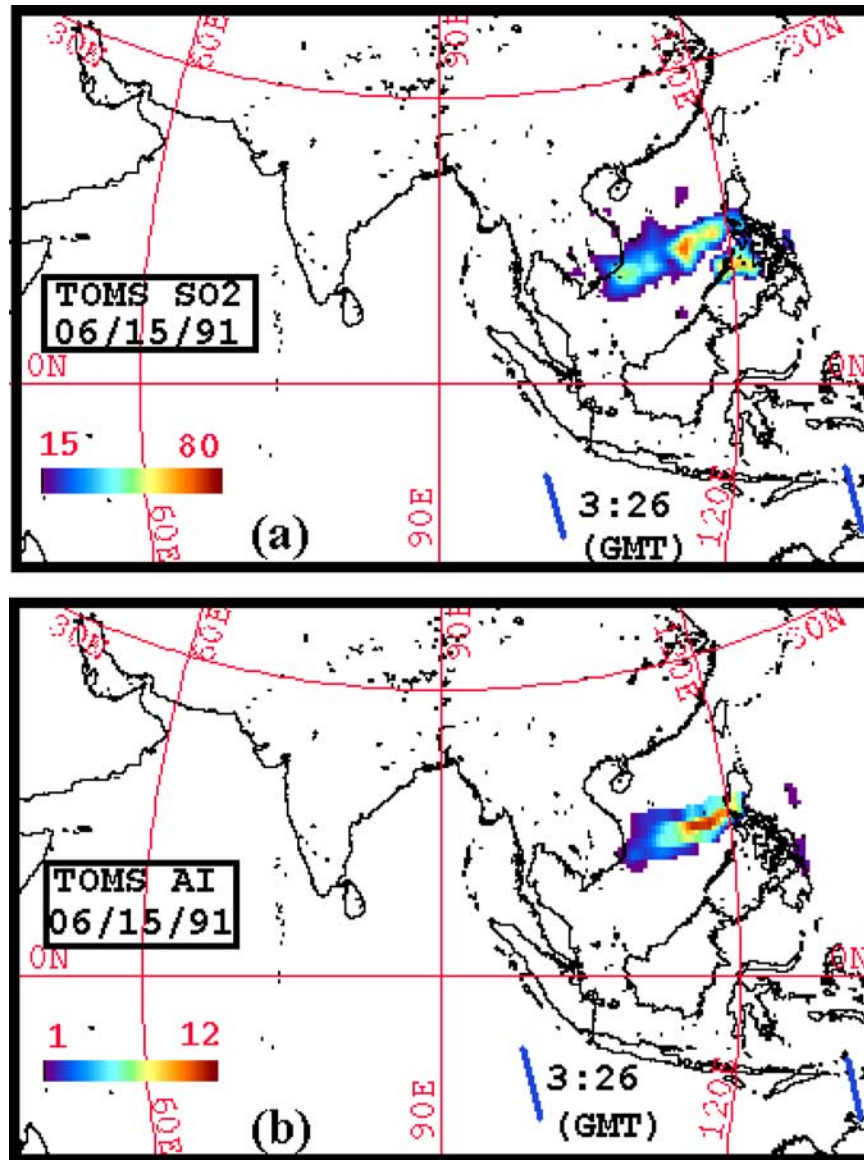


**Figure 5.** NASA TOMS maps: (a) SO<sub>2</sub> cloud map and (b) AI map, showing the SO<sub>2</sub> and ash clouds from the low-level activity before the climactic eruption at 05:41 (GMT) on 15 June. Latitude and longitude grid spacing is 30°. The SO<sub>2</sub> values are represented in Dobson Units (DU), and AI is unitless. The image sensing time is approximately the central pixel sensing time of the image in GMT as indicated in the figures.

used to distinguish volcanic clouds from meteorological clouds [Prata, 1989a]. Band 4 minus band 5 brightness temperature differences (BTD) usually have negative values for silicate particle dominated volcanic clouds [Prata, 1989a; Wen and Rose, 1994; Schneider *et al.*, 1999] and positive values for meteorological clouds [Yamanouchi *et al.*, 1987]. The reason for this difference is mainly due to the fact that silicate particles have a stronger dispersive nature than water/ice particles [Prata,

1989b]. The effective particle size, the optical depth of the volcanic cloud and the mass of fine ash or ice in the volcanic cloud can be retrieved by using the model developed by Wen and Rose [1994]. The maximum uncertainty for the AVHRR two-band split-window retrieval is 53% as summarized by Gu *et al.* [2003].

[10] However, owing to the high water vapor content in the moist tropical troposphere under

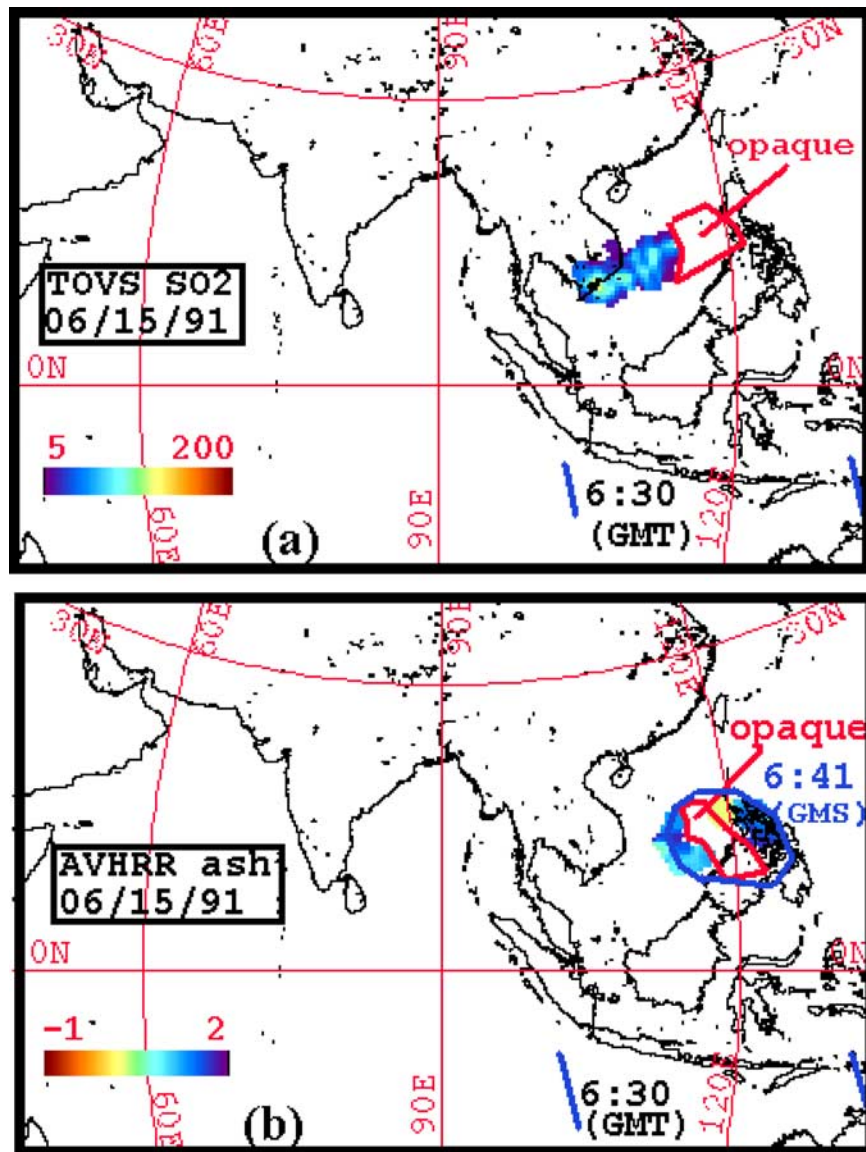


**Figure 6.** NOAA-11 maps: (a) TOVS SO<sub>2</sub> cloud map and (b) AVHRR BTd (ash cloud) map with atmospheric correction method [Yu *et al.*, 2002] applied. Latitude and longitude grid spacing is 30°. The SO<sub>2</sub> values are represented in Dobson Units (DU), and BTd values are represented in degrees Kelvin. The image sensing time is approximately the central pixel sensing time of the image in GMT as indicated in the figures.

the volcanic clouds, the BTd values of some ash particles (boundary, low BTd value regions) will be shifted to positive values [Yu *et al.*, 2002]. Thus only the central parts of volcanic clouds formed from Pinatubo can be detected by the traditional negative BTd retrieval scheme. An atmospheric moisture correction method, developed by Yu *et al.* [2002] to identify the ash-dominant pixels which might have a positive BTd value due to the water vapor interference, is used here. The atmospheric

moisture correction method uses both the BTd value and cloud temperature (T<sub>4</sub>) to identify the volcanic ash cloud.

[11] The ice retrieval used in this paper is based on Rose *et al.* [1995]. The theoretical calculated grid plots representing the look-up tables are calculated by using the same parameters in calculating the ash look-up tables, except the refractive index and density of ice are used.

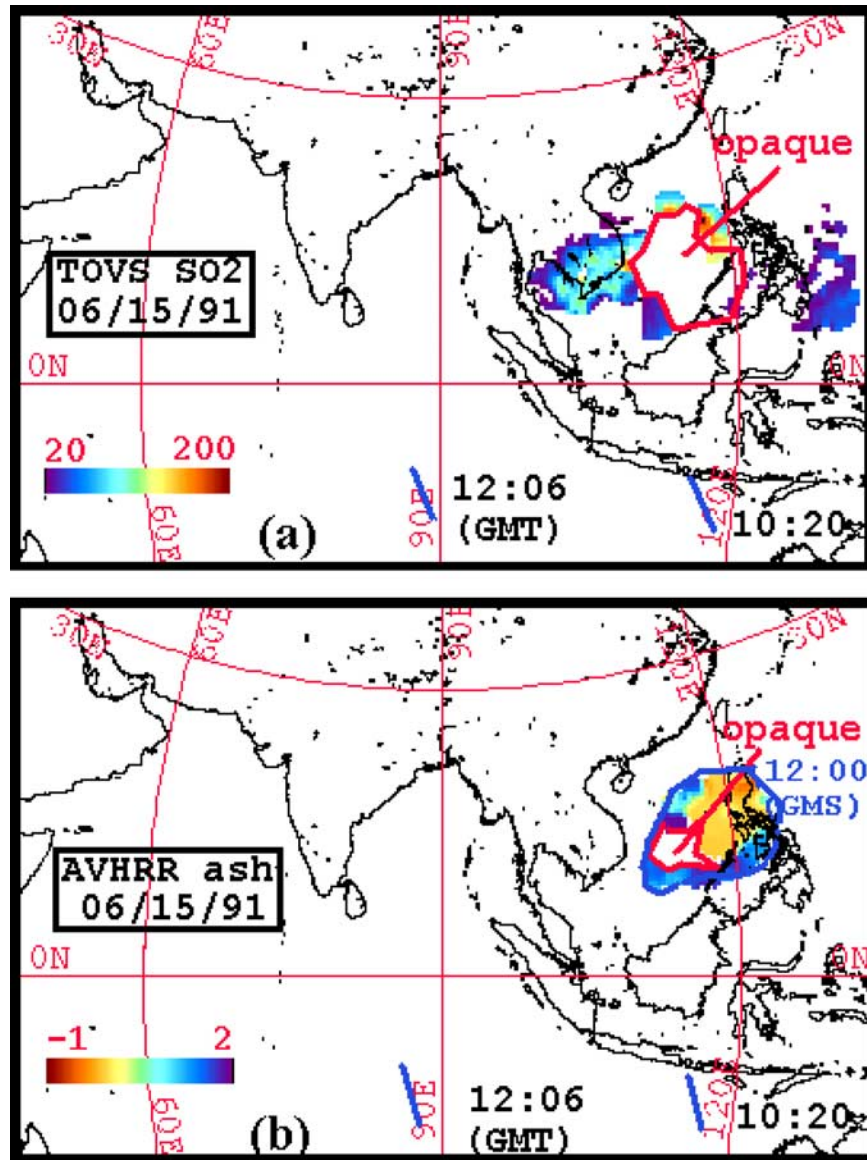


**Figure 7.** NOAA-12 maps: (a) TOVS SO<sub>2</sub> cloud map and (b) AVHRR BTDR (ash cloud) map with atmospheric correction method applied. Latitude and longitude grid spacing is 30°. The SO<sub>2</sub> values are represented in Dobson Units (DU), and BTDR values are represented in degrees Kelvin. The image sensing times are approximate the central pixel sensing time of the starting and ending orbits in GMT as indicated in the figures.

[12] In this paper, the volcanic ash is assumed to contain mainly andesite particles with 54% SiO<sub>2</sub> due to the availability of refractive indices for this composition. *Bernard et al.* [1996] found that most of the erupted magma was dacite, with 64.5% SiO<sub>2</sub>. The retrieval differences should be negligible based on the use of basalt (53.25% SiO<sub>2</sub>) and rhyolite (73.45% SiO<sub>2</sub>) for the comparison purpose. A lognormal particle size distribution with a standard deviation of 0.74 [Wen and Rose, 1994] is used. Both the andesite and ice particles are assumed

to be spherical, with densities of 2.6 g/cm<sup>3</sup> and 0.917 g/cm<sup>3</sup>, respectively [Neal *et al.*, 1994; Scott *et al.*, 1996]. The refractive indices of andesite and ice particles are based on Pollack *et al.* [1973] and Kou *et al.* [1993].

### 3.3. HIRS/2 Multiband Retrieval

[13] A multiband retrieval using six infrared bands (bands 5–10) of HIRS/2 data were used for estimates (optical depth, effective radius, mass) of ice,

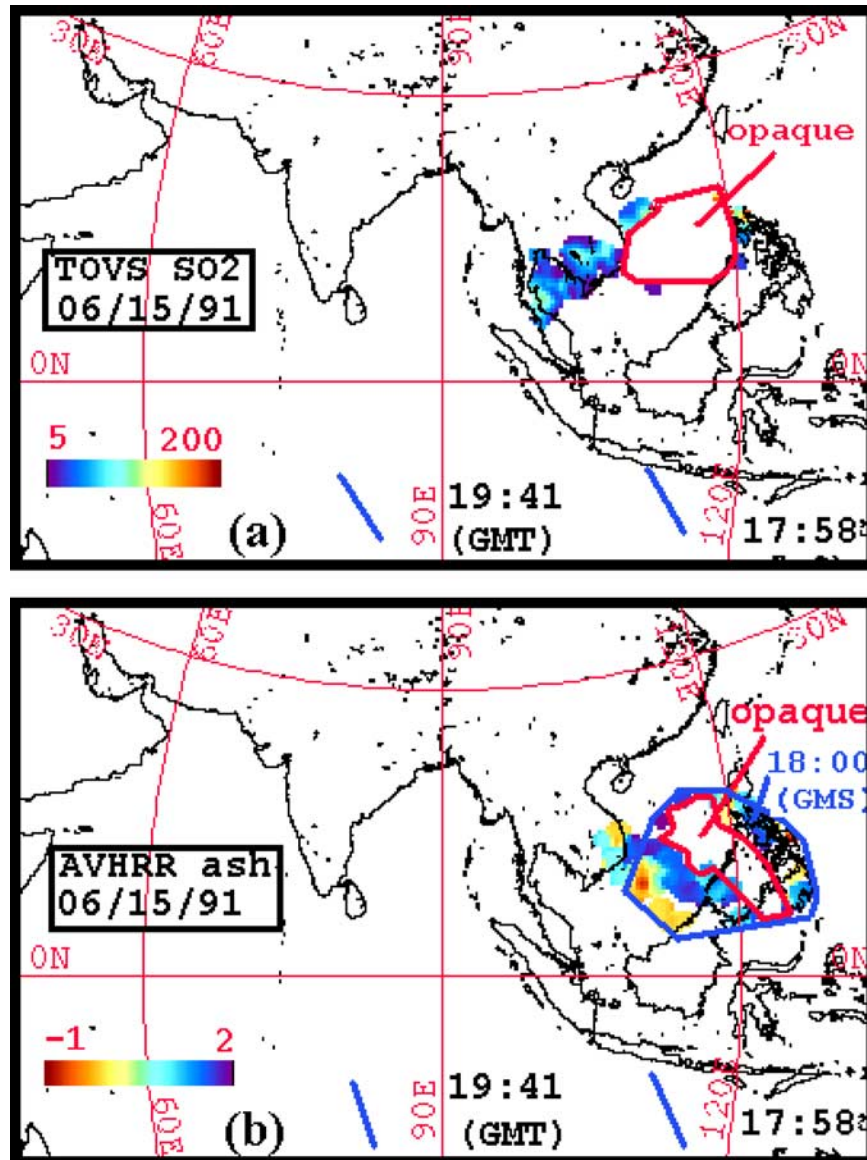


**Figure 8.** NOAA-11 maps: (a) TOVS SO<sub>2</sub> cloud map and (b) AVHRR BTM (ash cloud) map with atmospheric correction method applied. Latitude and longitude grid spacing is 30°. The SO<sub>2</sub> values are represented in Dobson Units (DU), and BTM values are represented in degrees Kelvin. The image sensing times are approximately the central pixel sensing time of the starting and ending orbits in GMT as indicated in the figures.

ash and sulfate particles in the Pinatubo volcanic clouds, following the work of *Yu and Rose* [2000]. The retrieval compares observed HIRS/2 radiances with a lookup table of simulated values based on MODTRAN [*Berk et al.*, 1989] calculations of volcanic clouds containing reference mixtures of particles at the same heights of the Pinatubo cloud. We further improved the calculations of simulated cloud particle mixtures for this study by using a forward model developed by *Watson et al.* [2003],

which can calculate spectral transmission through volcanic clouds caused by different solid species, or mixtures of species. SO<sub>2</sub> cloud maps from TOMS and TOVS data, ash cloud maps from AVHRR, and TOMS AI are used to select volcanic cloud areas to carry out multiband retrievals using HIRS/2 data. The ice, ash and sulfate particles in each forward model calculation are assumed to be spherical and of uniform size. A total of 144, 627 unique mixtures of ice, ash and sulfate were examined systematically

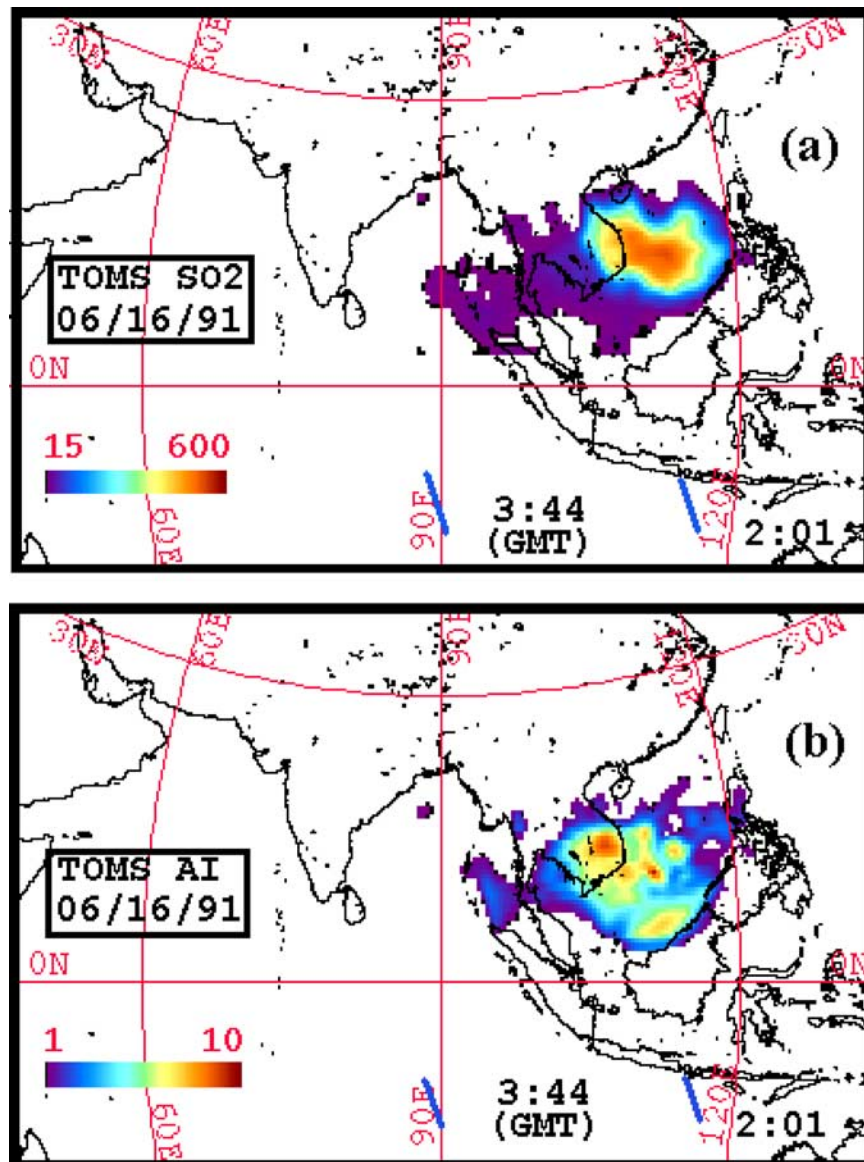


**Figure 9.** NASA TOMS maps: (a) SO<sub>2</sub> cloud map and (b) AI map. Latitude and longitude grid spacing is 30°. The SO<sub>2</sub> values are represented in Dobson Units (DU), and AI is unitless. The image sensing times are approximately the central pixel sensing time of the starting and ending orbits in GMT as indicated in the figures.

using typical size values for each species (diameter ranges of 1–30 microns for ice, 1–15 microns for ash, and 0.1 to 0.5 microns for sulfate). A non-negative least squares analysis is then used to search for the most compatible results, and this is shown graphically for two-component mixtures for one of the Pinatubo clouds in Figures 1 and 2. The method produces a pronounced minimum of likely ice and ash proportions (Figure 2a) and a weak minimum for mixtures involving sulfate (Figures 2b and 2c). Refractive index data for

andesite determined by *Pollack et al.* [1973] was used for the Pinatubo ash. *Yu and Rose* [2000] investigated and discussed the errors involved in this method. The assumption of spherical size for particles is incorrect, and the implications of this are not explored here. *Riley et al.* [2003] have shown that basaltic and andesitic volcanic ash is more nearly spherical (aspect ratio of 1.5–1.7) than rhyolitic ash (aspect ratio of 2.2), but the effects of this on radiative transfer are uncertain. The assumption of uniform size was determined to have

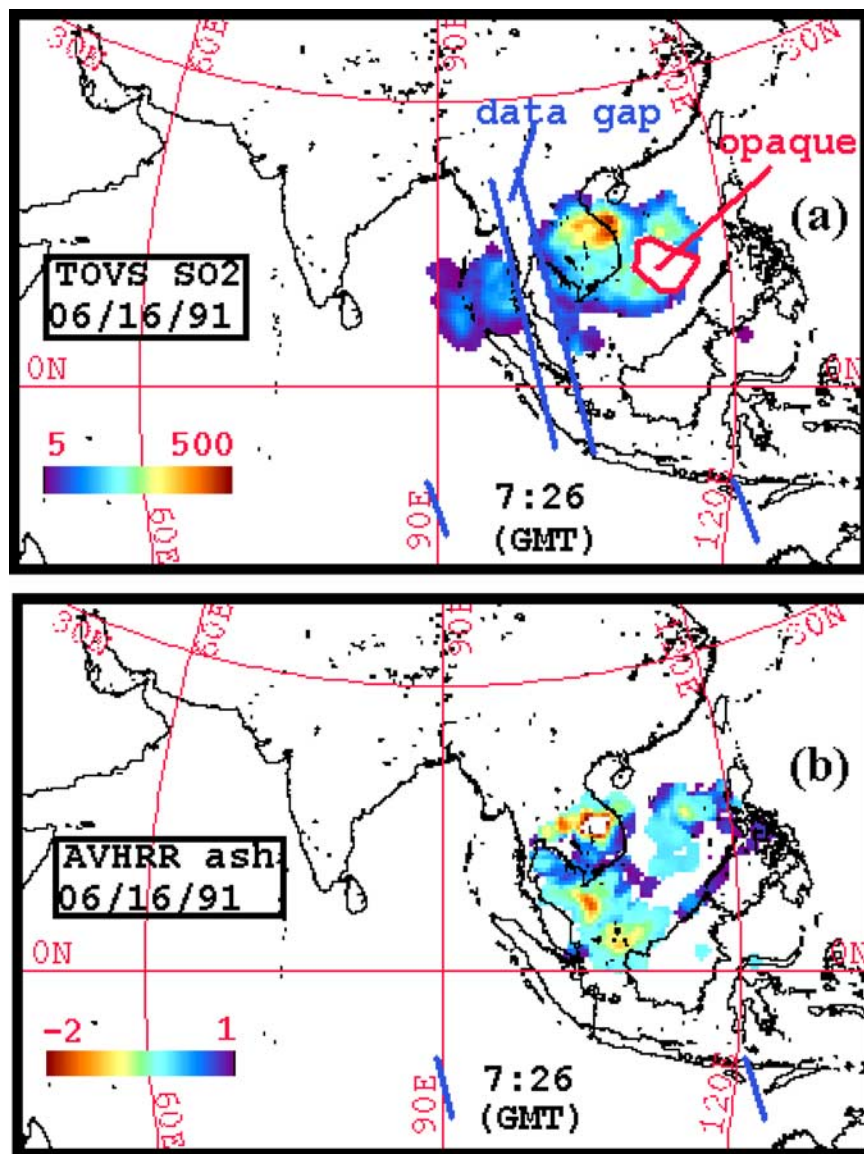


**Figure 10.** NOAA-11 maps: (a) TOVS SO<sub>2</sub> cloud map and (b) AVHRR BTM (ash cloud) map with atmospheric correction method applied. Latitude and longitude grid spacing is 30°. The SO<sub>2</sub> values are represented in Dobson Units (DU), and BTM values are represented in degrees Kelvin. The image sensing times are approximately the central pixel sensing time of the starting and ending orbits in GMT as indicated in the figures.

a significant impact by causing an overall underestimate of mass by approximately 30–40%. The assumption of negligible scattering is also debatable and untested. The mean (and maximum) uncertainties for the HIRS/2 multiband retrieved effective radius, optical depth are 40 (60)%, and 30 (45)%, respectively for ash and ice, and higher for sulfate [Yu and Rose, 2000]. Mass estimates are of course based on both the radius and optical depth estimates and therefore have larger errors. Overall

there is much uncertainty in this technique and it is discussed much more by Yu and Rose [2000]. Usually, although both AVHRR and HIRS-2 data are available on volcanic clouds from polar-orbiting NOAA satellites, we use two band AVHRR data for ash estimates. In this paper, however, we have used HIRS-2 simultaneous retrievals of the properties of silicate ash, ice, and sulfate particles because ash, ice, and/or particles that are mixtures of the two are thought to coexist with sulfate in the Pinatubo

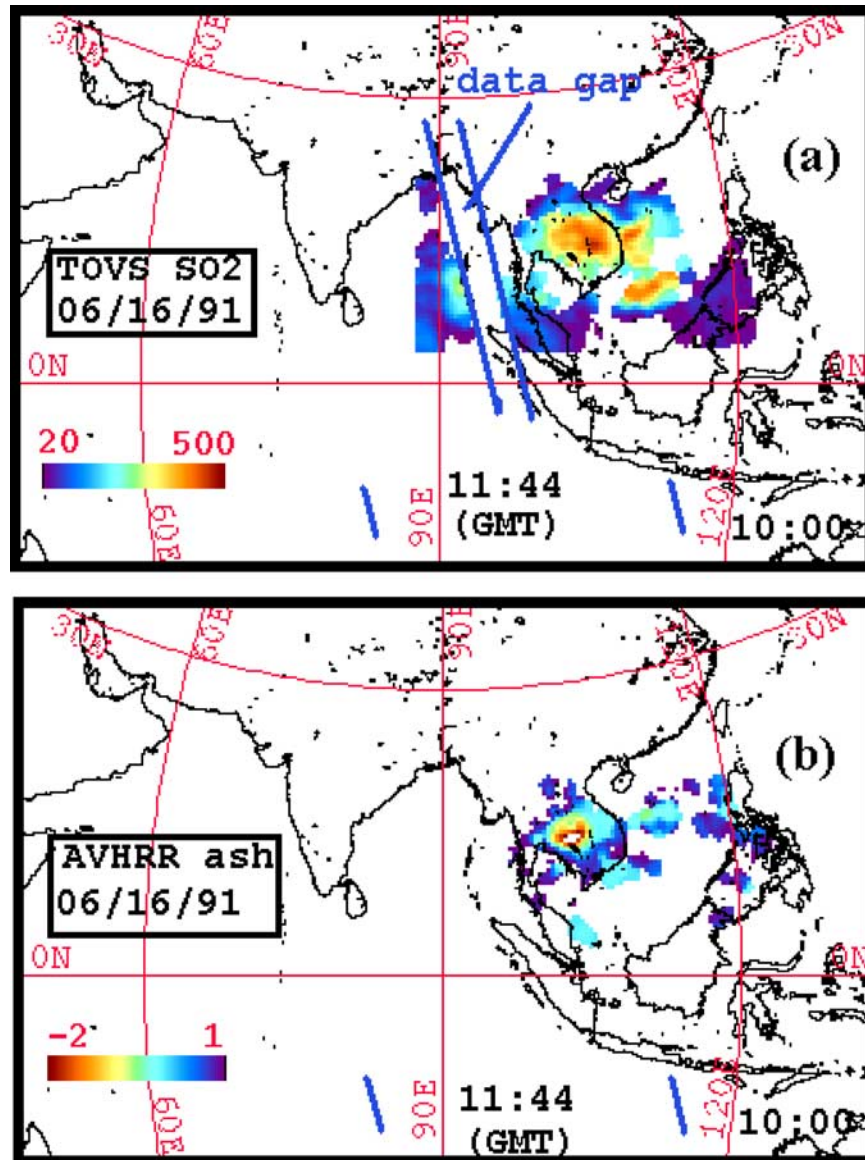


**Figure 11.** NOAA-12 maps: (a) TOVS SO<sub>2</sub> cloud map and (b) AVHRR BTD (ash cloud) map with atmospheric correction method applied. Latitude and longitude grid spacing is 30°. The SO<sub>2</sub> values are represented in Dobson Units (DU), and BTD values are represented in degrees Kelvin. The image sensing times are approximately the central pixel sensing time of the starting and ending orbits in GMT as indicated in the figures.

cloud and this precludes meaningful two band retrievals.

### 3.4. Wind Trajectory Modeling

[14] An isentropic wind trajectory model developed by scientists from NASA GSFC (Goddard Space Flight Center) [Schoeberl *et al.*, 1992, 1993] is used in this study to estimate cloud height. Shannon [1997] used the NASA wind trajectory model to view the drifting of volcanic gas clouds in

three dimensions. By comparing cloud positions derived from the satellite sensors, the NASA wind trajectory model can constrain the height of volcanic cloud, which is needed in retrieval algorithms. The atmospheric temperature and wind (direction and speed) profiles at different locations (grid points of the model domain) are the key inputs to run the trajectory model. No real time atmospheric sounding data were found within 500 miles around Mt. Pinatubo during the eruption period in the GSFC DAO (Data Assimilation Office) or

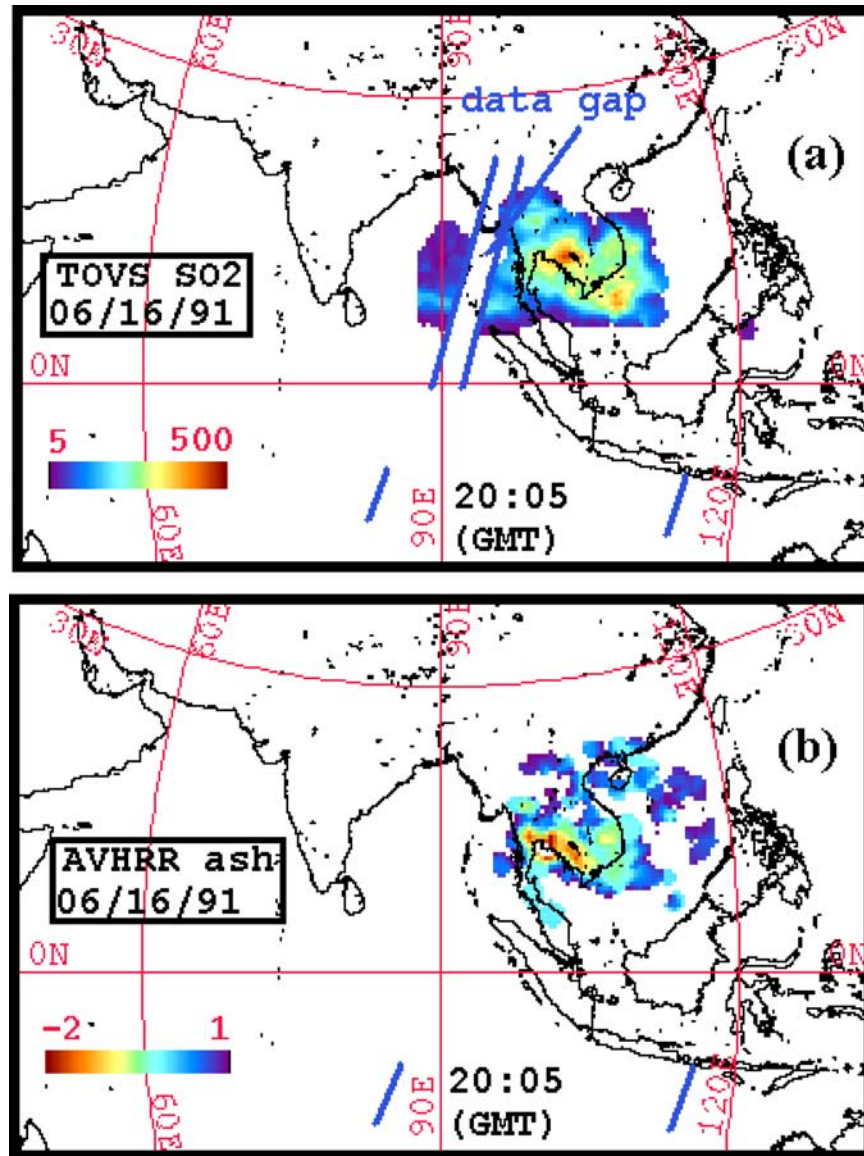


**Figure 12.** NOAA-11 maps: (a) TOVS SO<sub>2</sub> cloud map and (b) AVHRR BTDR (ash cloud) map with atmospheric correction method applied. Latitude and longitude grid spacing is 30°. The SO<sub>2</sub> values are represented in Dobson Units (DU), and BTDR values are represented in degrees Kelvin. The image sensing times are approximately the central pixel sensing time of the starting and ending orbits in GMT as indicated in the figures.

UARS UKMO (UK Meteorological Office) databases. Therefore the inputs are based primarily on the NCEP/NCAR (National Center for Environmental Prediction/National Center for Atmospheric Research) Reanalysis data set [McPherson *et al.*, 1979].

### 3.5. Other Cloud Maps Used in the Paper

[15] TOVS and TOMS SO<sub>2</sub> maps are also used in this paper for SO<sub>2</sub> cloud height estimation, through comparison with the wind trajectory results

at different levels between 20 and 30 km. The generation of TOMS and TOVS SO<sub>2</sub> maps are described in detail by Guo *et al.* [2004].

## 4. Results

### 4.1. Coexistence of Ash and Ice in the Pinatubo Cloud

[16] Pinatubo's volcanic clouds differ from other volcanic clouds seen with IR sensors as described below. Figure 3 shows the BTDR (brightness tem-

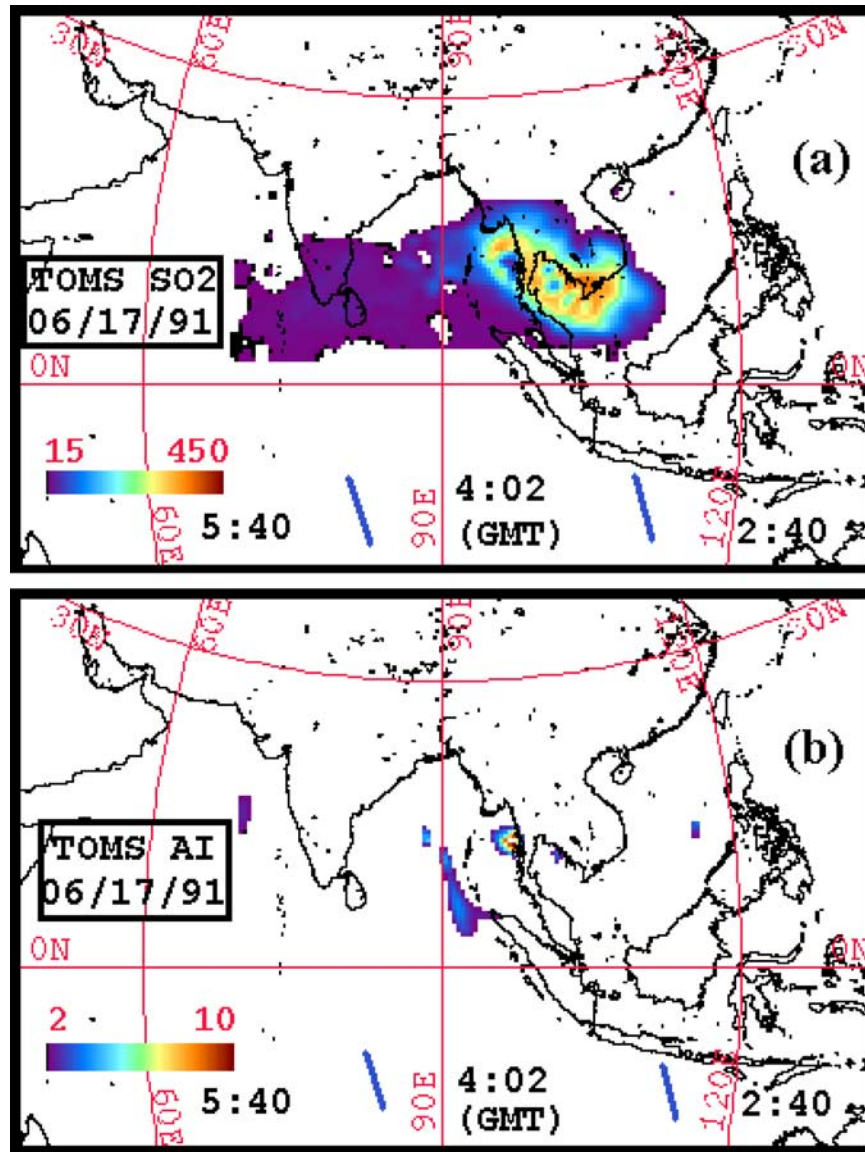


**Figure 13.** NASA TOMS maps: (a) SO<sub>2</sub> cloud map and (b) AI map. A tiny amount of ash signals appears on the AI map, which might be due to the increase of sulfate aerosol within the cloud (see discussion in text). Latitude and longitude grid spacing is 30°. The SO<sub>2</sub> values are represented in Dobson Units (DU), and AI is unitless. The image sensing times are approximately the central pixel sensing time of the starting and ending orbits in GMT as indicated in the figures.

perature differences of band 4 and 5) versus T4 (band 4 brightness temperature) plot of the 16 June 07:28 (GMT) AVHRR ash map (Figure 3). Similar patterns of BTD versus T4 were found for the other 13 AVHRR Pinatubo ash maps during the first five days after eruption. A majority of pixels have positive BTD values, which, together with the low temperatures, are consistent with the presence of significant ice within the volcanic cloud. The

region labeled “ice-region” (BTD > 3.0) reflects pixels dominated by ice. The BTD = 3.0 line represents the maximum BTD value of “clear air” pixels over the tropical ocean [Yu *et al.*, 2002]. Pixels with BTD < 0 reflect the influence of volcanic ash. The triangular region bounded by points B, C, and D, which have BTD values between 0.0 and 3.0 and T4 values between 250 and 280, is the atmospheric correction region for

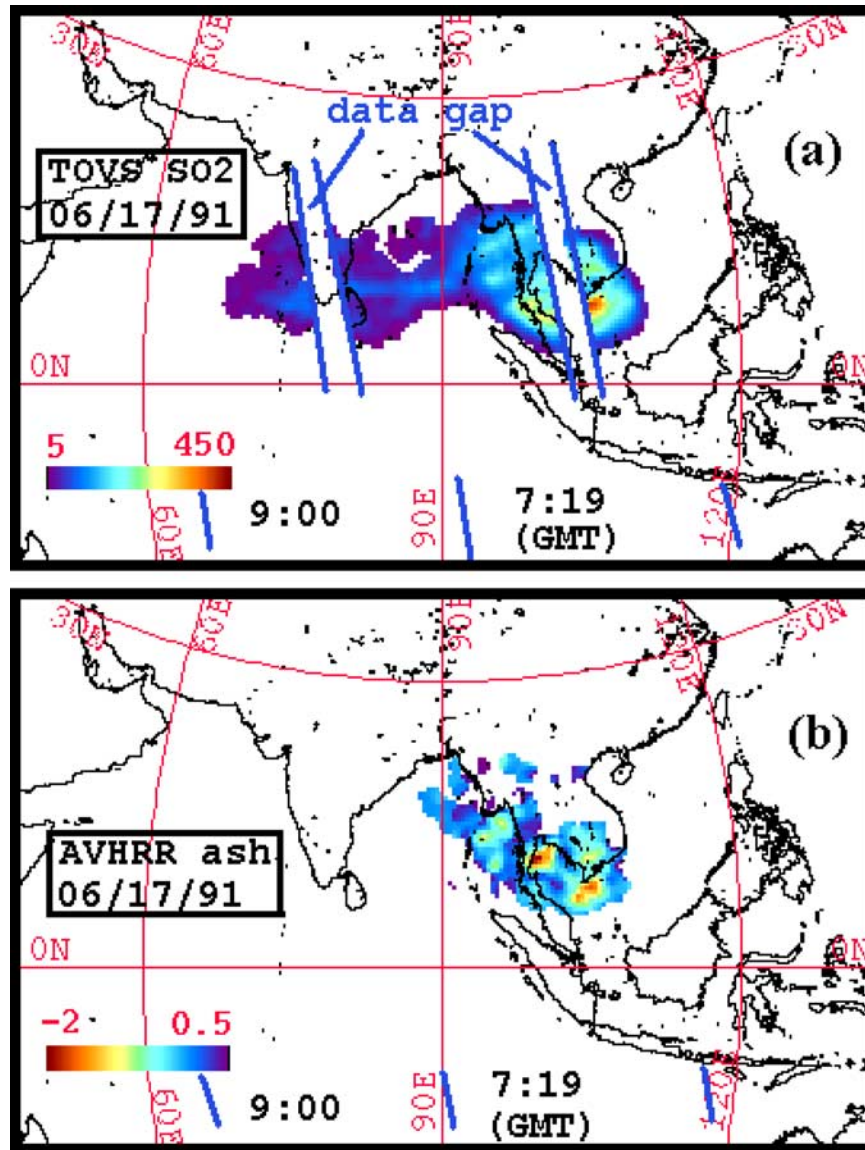


**Figure 14.** NOAA-11 maps: (a) TOVS SO<sub>2</sub> cloud map and (b) AVHRR BTM (ash cloud) map with atmospheric correction method applied. Latitude and longitude grid spacing is 30°. The SO<sub>2</sub> values are represented in Dobson Units (DU), and BTM values are represented in degrees Kelvin. The image sensing times are approximately the central pixel sensing time of the starting and ending orbits in GMT as indicated in the figures.

volcanic ash using the *Yu et al.* [2002] method. This region is dominated by ash and the shift of BTM value to values >0 is caused by lower tropospheric water vapor and very low optical depth. Pixels whose BTM values are between 0.0 and 3.0 and outside the atmospherically corrected triangle region are interpreted as “mixtures” of ash and ice (ash-ice hybrid, ash nucleated ice particles, and pure hydrometeors). Two analogous plots from *Rose et al.* [1995] are presented again in this paper

to show patterns seen in ash-dominated and ice-dominated volcanic clouds, respectively (Figure 4). Figure 4a is the retrieval grid of the 19 September Rabaul (Papua, New Guinea) volcanic cloud at 09:00 (GMT), showing the ice-dominated volcanic cloud which mainly has positive BTM values. Figure 4b is the retrieval grid of the 1 October 1994 Klyuchevskoi (Kamchatka, Russia) volcanic cloud at 06:40 (GMT), showing the ash-dominated volcanic cloud with mainly negative BTM values.

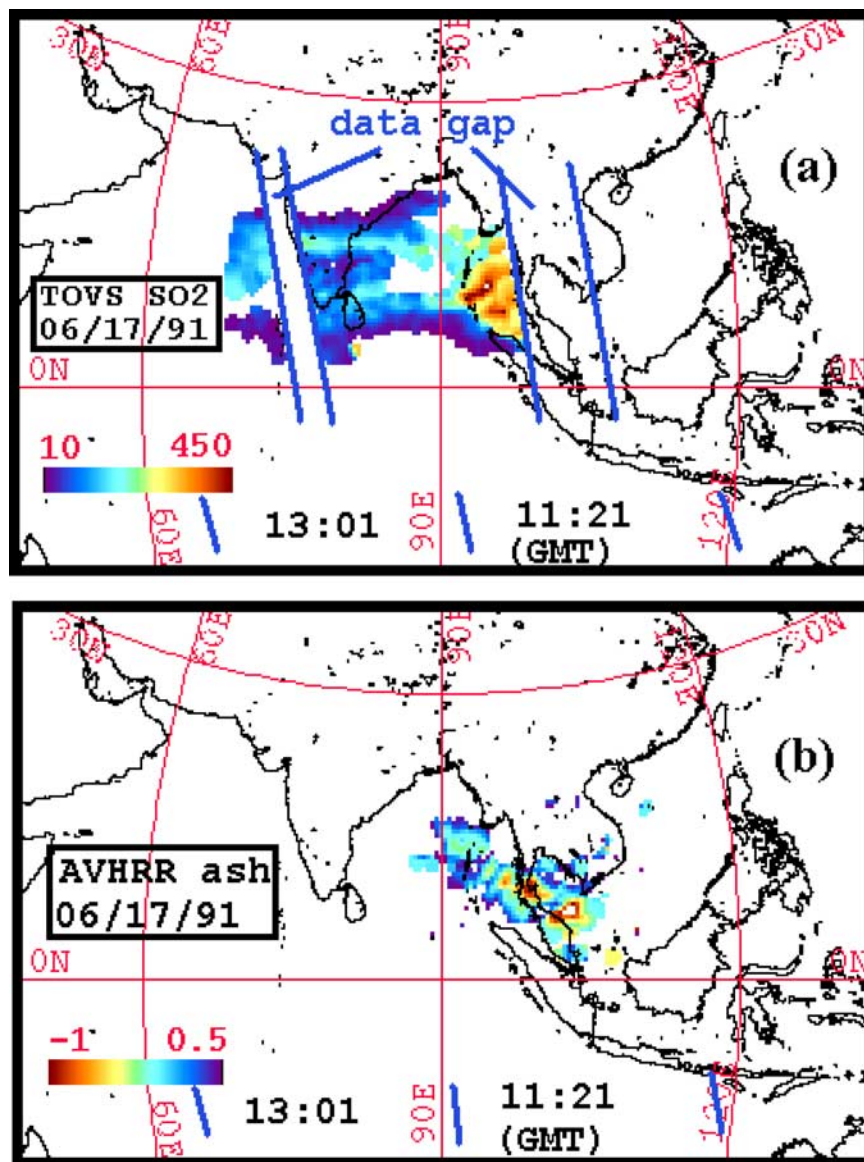


**Figure 15.** NOAA-12 maps: (a) TOVS SO<sub>2</sub> cloud map and (b) AVHRR BTD (ash cloud) map with atmospheric correction method applied. Latitude and longitude grid spacing is 30°. The SO<sub>2</sub> values are represented in Dobson Units (DU), and BTD values are represented in degrees Kelvin. The image sensing times are approximately the central pixel sensing time of the starting and ending orbits in GMT as indicated in the figures.

Through comparison, we conclude that Pinatubo clouds contain ice, ash and perhaps the mixtures of the two (hybrid mixtures, or icy ash balls, or ash nucleated icy balls) and the signals seen in the two-band retrieval reflect hybrids of ash and ice. This indicates that the ash retrievals done with AVHRR data are unlikely to be as useful as they have been for other eruptions, because we cannot assume that ice has no effect on the BTD values. More work is needed in the future in the conflicting effects of ash and ice in the AVHRR two-band retrievals.

[17] An abundance of H<sub>2</sub>O sources also makes the coexistence of ash and ice within Pinatubo cloud possible. *Rutherford and Devine* [1996] point out that for Pinatubo, 5.1 to 6.4 percent of the preeruption magma is H<sub>2</sub>O. If the total erupted bulk volume of 8.4–10.4 km<sup>3</sup> [*Scott et al.*, 1996] and bulk density of 1.5 g/cm<sup>3</sup> [*Scott et al.*, 1996] are used, then the magma released 643–998 Mt H<sub>2</sub>O. *Gerlach et al.* [1996] estimate a maximum of 491–921 Mt water in the erupted plume based on both modeling of the composi-

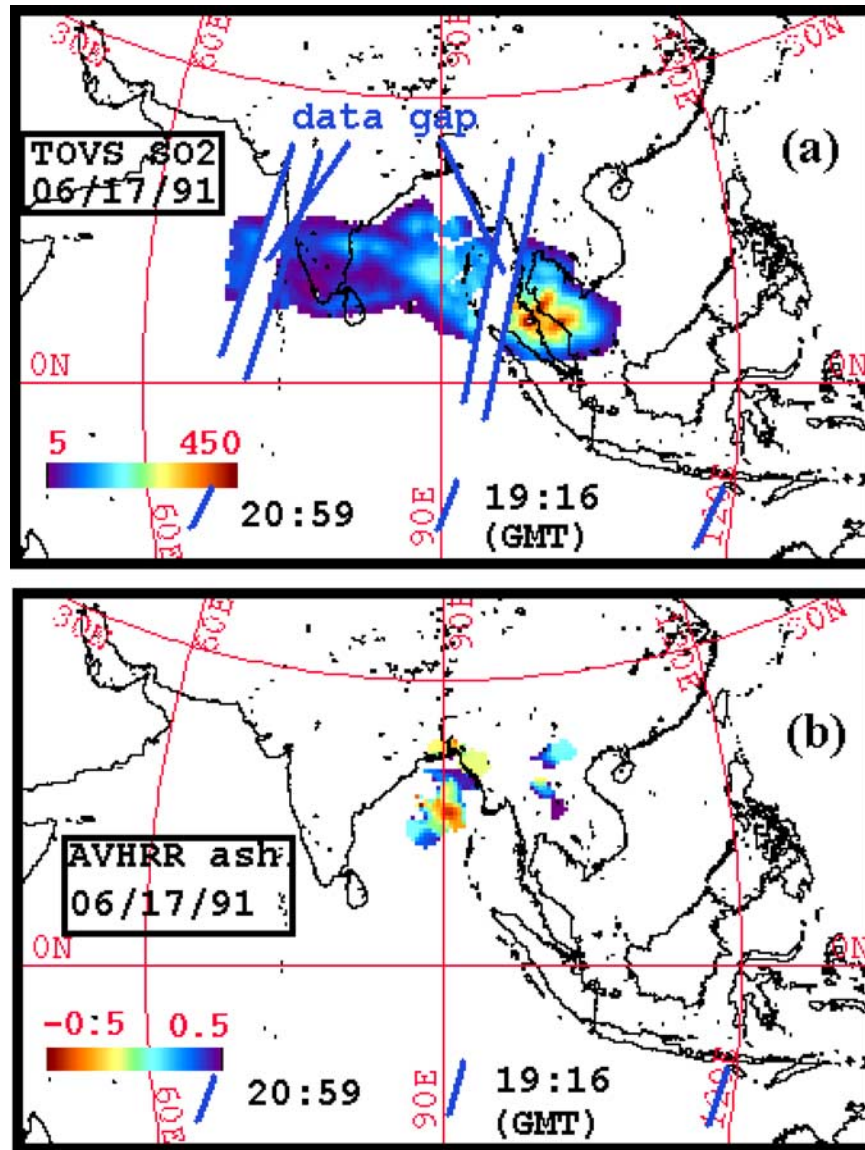


**Figure 16.** NOAA-11 maps: (a) TOVS SO<sub>2</sub> cloud map and (b) AVHRR BTDR (ash cloud) map with atmospheric correction method applied. Latitude and longitude grid spacing is 30°. The SO<sub>2</sub> values are represented in Dobson Units (DU), and BTDR values are represented in degrees Kelvin. The image sensing times are approximately the central pixel sensing time of the starting and ending orbits in GMT as indicated in the figures. Detection of the movement of volcanic clouds is interfered with by a tropical cyclone developed in the Bay area between Thailand and India.

tion of the pre-eruption vapor and degassing of melts. The Pinatubo plume likely also entrained abundant H<sub>2</sub>O from a very moist tropical atmosphere as suggested by numerical simulation conducted by ATHAM (Active Tracer High Resolution Atmospheric Model) [Herzog *et al.*, 1998; Guo *et al.*, 2000]. The Pinatubo volcanic cloud was also fed from significant co-ignimbrite cloud formation which can further enhance entrainment [Darteville *et al.*, 2002]. In addition,

there was an active tropical cyclone, Typhoon Yunya, passing the Pinatubo area during the eruption period. Thus very large amounts of water vapor were convected with the volcanic cloud which likely led to significant amounts of ice, enough to overwhelm the effects of ash. The various sources of H<sub>2</sub>O can not be individually assessed in this study, but the larger ice proportions mean that the two-band ash retrieval could not be reliably used alone to estimate ash

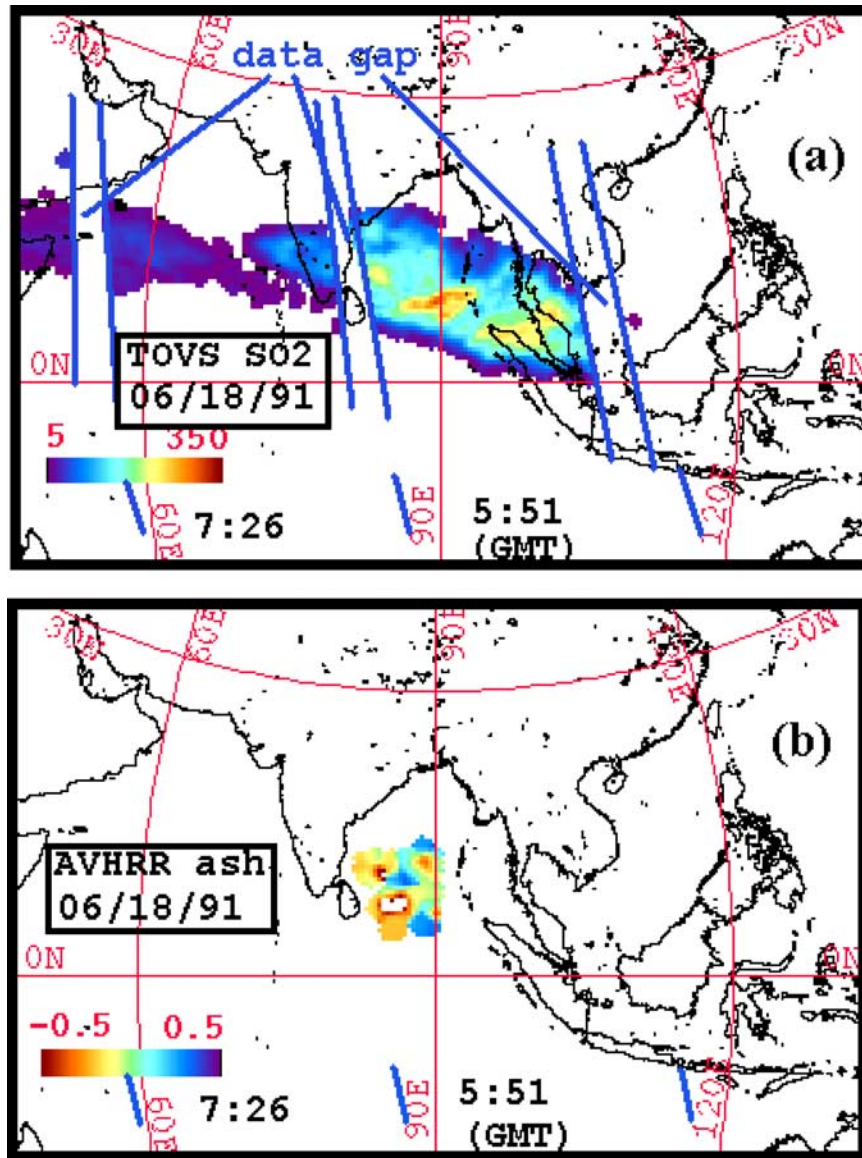


**Figure 17.** NOAA-11 maps: (a) TOVS SO<sub>2</sub> cloud map and (b) AVHRR BTDR (ash cloud) map with atmospheric correction method applied. Latitude and longitude grid spacing is 30°. The SO<sub>2</sub> values are represented in Dobson Units (DU), and BTDR values are represented in degrees Kelvin. The image sensing times are approximately the central pixel sensing time of the starting and ending orbits in GMT as indicated in the figures. Detection of the movement of volcanic clouds is interfered with by a tropical cyclone developed in the Bay area between Thailand and India.

masses, and ash maps based on this method are also inadequate.

#### 4.2. Two-Dimensional Maps of the Pinatubo Ash and SO<sub>2</sub> Clouds

[18] In spite of the problems presented by ice, we mapped the two-dimensional (2-D) distribution of the Pinatubo ash clouds using two-band AVHRR BTDR maps for several days after the 15 June 1991 eruption. We also used TOMS AI data for mapping

ash clouds, because we think that presence of ice causes the AVHRR maps to underestimate 2-D areas. We compare these ash maps with SO<sub>2</sub> maps derived from TOVS and TOMS at the same time to compare the cloud areas and positions (Figures 5–21, Animations 1 and 2). Overall these maps demonstrate that SO<sub>2</sub> persists in the cloud much longer than volcanic ash and the area represented by ash-dominant pixels decreases strongly after 24 hours and is 20% of its maximum after

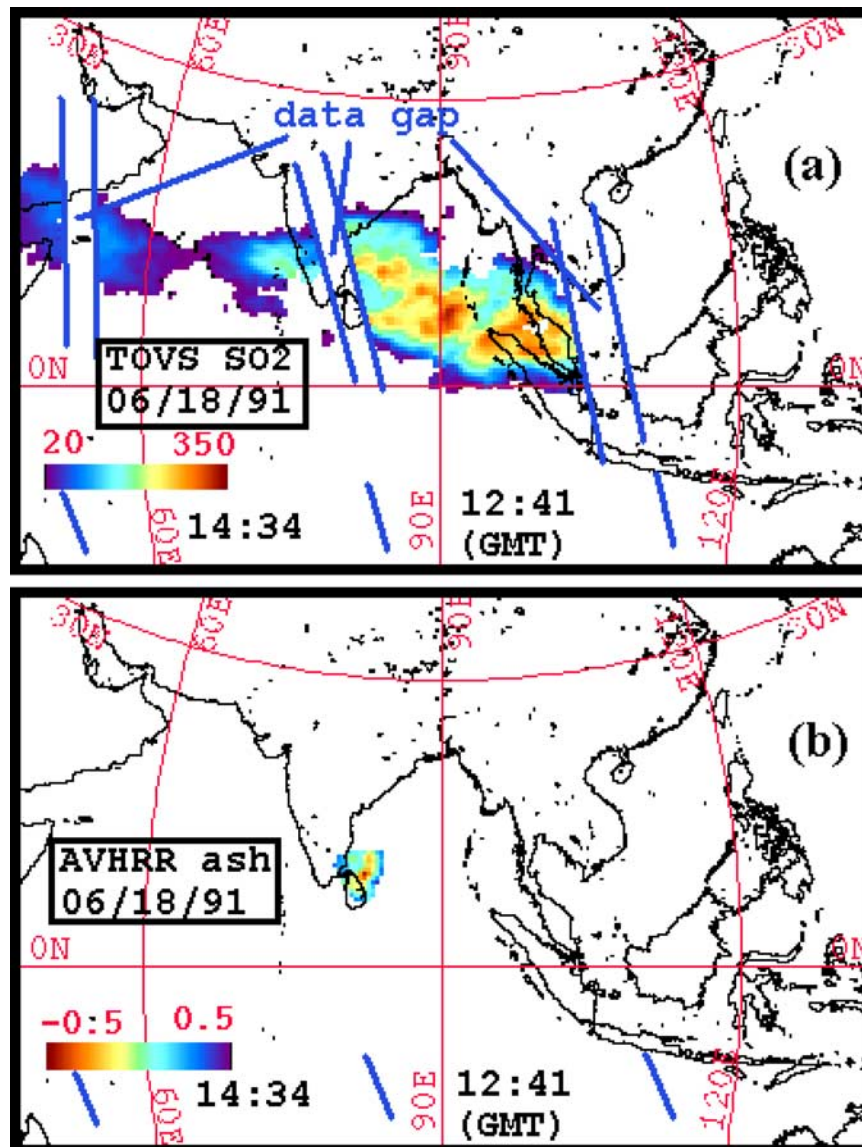


**Figure 18.** NOAA-12 maps: (a) TOVS SO<sub>2</sub> cloud map and (b) AVHRR BTDR (ash cloud) map with atmospheric correction method applied. Latitude and longitude grid spacing is 30°. The SO<sub>2</sub> values are represented in Dobson Units (DU), and BTDR values are represented in degrees Kelvin. The image sensing times are approximately the central pixel sensing time of the starting and ending orbits in GMT as indicated in the figures.

70 hours (Figure 23). Because of the dominating effects of ice, the areas shown in the AVHRR maps likely underestimate the area where ash exists in the volcanic cloud.

[19] These maps offer little evidence that SO<sub>2</sub>-rich and ash-rich portions of the Pinatubo volcanic cloud separated as they did in the case of El Chichón in 1982 [Schneider *et al.*, 1999]. SO<sub>2</sub> clouds may be traveling to the west slightly faster than ash (Figures 6–21), due to the fact that wind

directions at all levels in the stratosphere are consistently easterly but intensities increase with altitude above the tropopause (Figure 27).

#### 4.3. Ash Retrievals Using the AVHRR Split-Window and HIRS/2 Multibands

[20] The mean particle effective radius, the optical depth of the volcanic cloud and the mass of fine ash were retrieved for each AVHRR map using the retrieval model developed by Wen and Rose

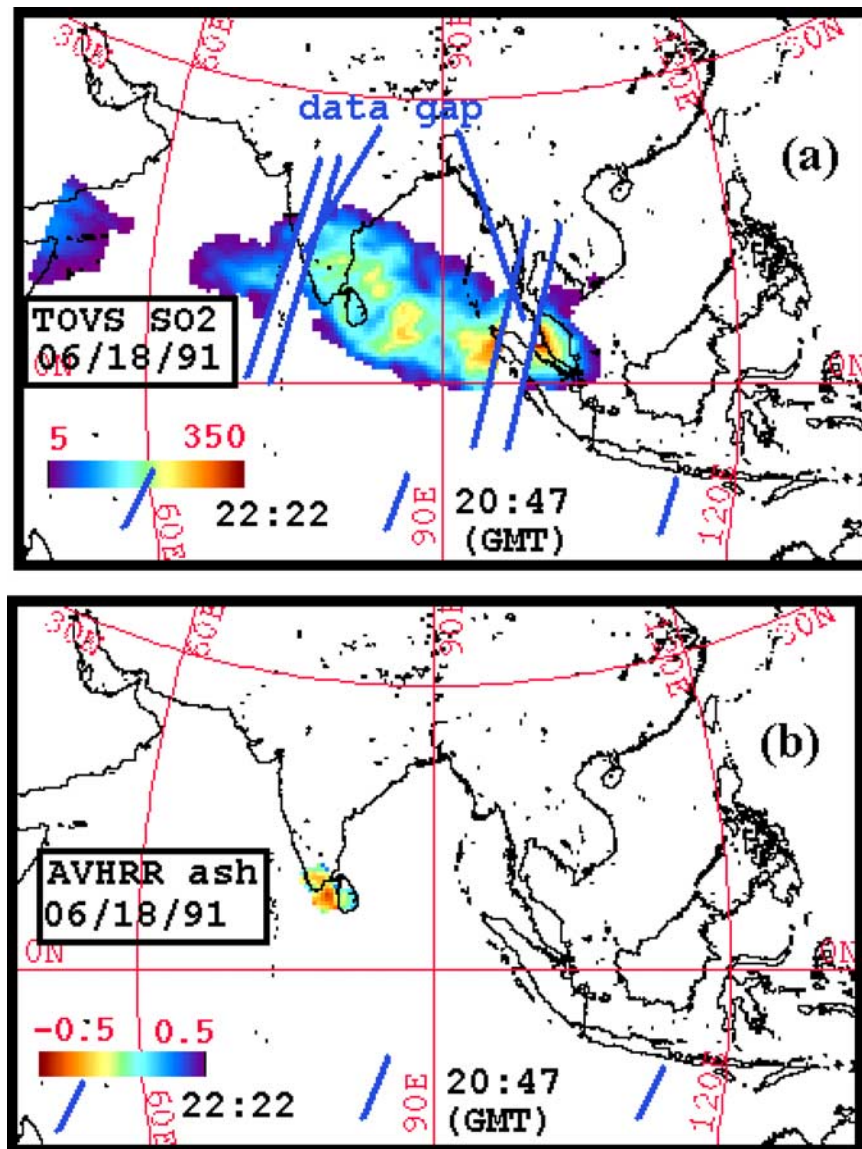


**Figure 19.** NOAA-11 maps: (a) TOVS SO<sub>2</sub> cloud map and (b) AVHRR BTD (ash cloud) map with atmospheric correction method applied. Latitude and longitude grid spacing is 30°. The SO<sub>2</sub> values are represented in Dobson Units (DU), and BTD values are represented in degrees Kelvin. The image sensing times are approximately the central pixel sensing time of the starting and ending orbits in GMT as indicated in the figures.

[1994] (Table 3), giving us data to assess changes of ash particles during the first few days of the Pinatubo volcanic cloud. The atmospheric correction method developed by *Yu et al.* [2002] was applied to retrievals due to the moist tropical troposphere (high water vapor contents below the volcanic ash cloud). The BTD cutoff values, band 4 and band 5 temperatures of underlying surface, and cloud temperatures used in the atmospheric correction method are summarized in Table 4. Opaque cloud areas exist in the AVHRR

ash images collected during the first 20 hours after eruption, so that the retrieved fine ash mass for these images are only lower limits of the volcanic fine ash mass for the first 20 hours after eruption.

[21] Simultaneous retrievals of ash, ice and sulfate properties (mass, mean effective radius, optical depth) were conducted using HIRS/2 data and a sulfate and silicate ash retrieval model developed by *Yu and Rose* [2000]. Because they are based on

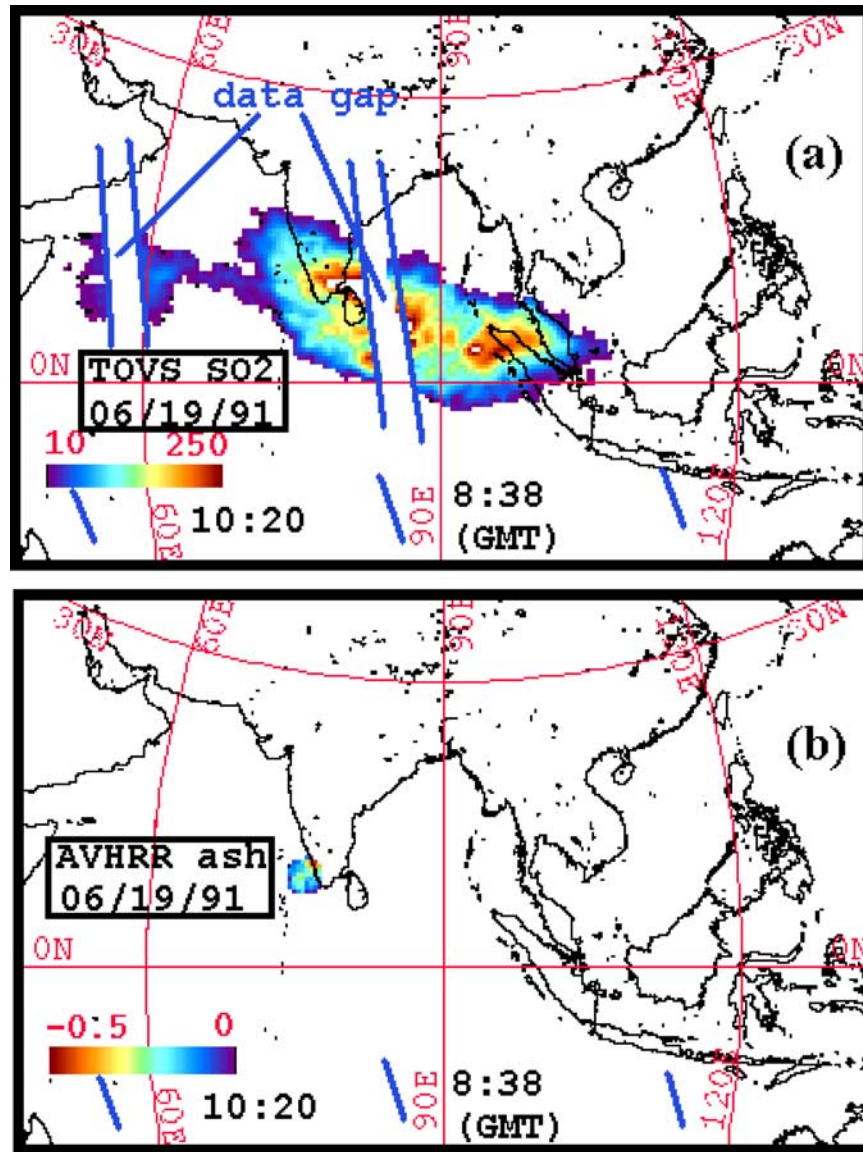


**Figure 20.** NOAA-11 maps: (a) TOVS SO<sub>2</sub> cloud map and (b) AVHRR BTDR (ash cloud) map with atmospheric correction method applied. Latitude and longitude grid spacing is 30°. The SO<sub>2</sub> values are represented in Dobson Units (DU), and BTDR values are represented in degrees Kelvin. The image sensing times are approximately the central pixel sensing time of the starting and ending orbits in GMT as indicated in the figures.

multiband data and retrieve all three particle types simultaneously, the HIRS/2 results are probably more robust and more indicative of what really happened. Figure 1 shows the best fit, calculated optical depth curves for mixtures of ash, ice, and sulfate and mixtures of ash and sulfate with observed optical depths at different wavelengths. It shows that sulfate particles contribute less to the total optical depth than ash and ice particles. Figure 2 is best fit residual surface graph showing differences between observed and calculated opti-

cal depths based on all combinations of ash, ice, and sulfate particle sizes using the whole look-up table. It indicates that sulfate particle size selection has the least influence on the residual. Thus accurate retrievals of sulfate properties are more problematic than those of ash and ice. Figures 1 and 2 are meant to give the reader insight into the multiband retrieval. Simultaneous retrievals of particle properties (effective radius, optical depth, mass) of fine ash (1–15 μm), fine ice (or ash covered by ice) (1–30 μm), and sulfate (0.1–

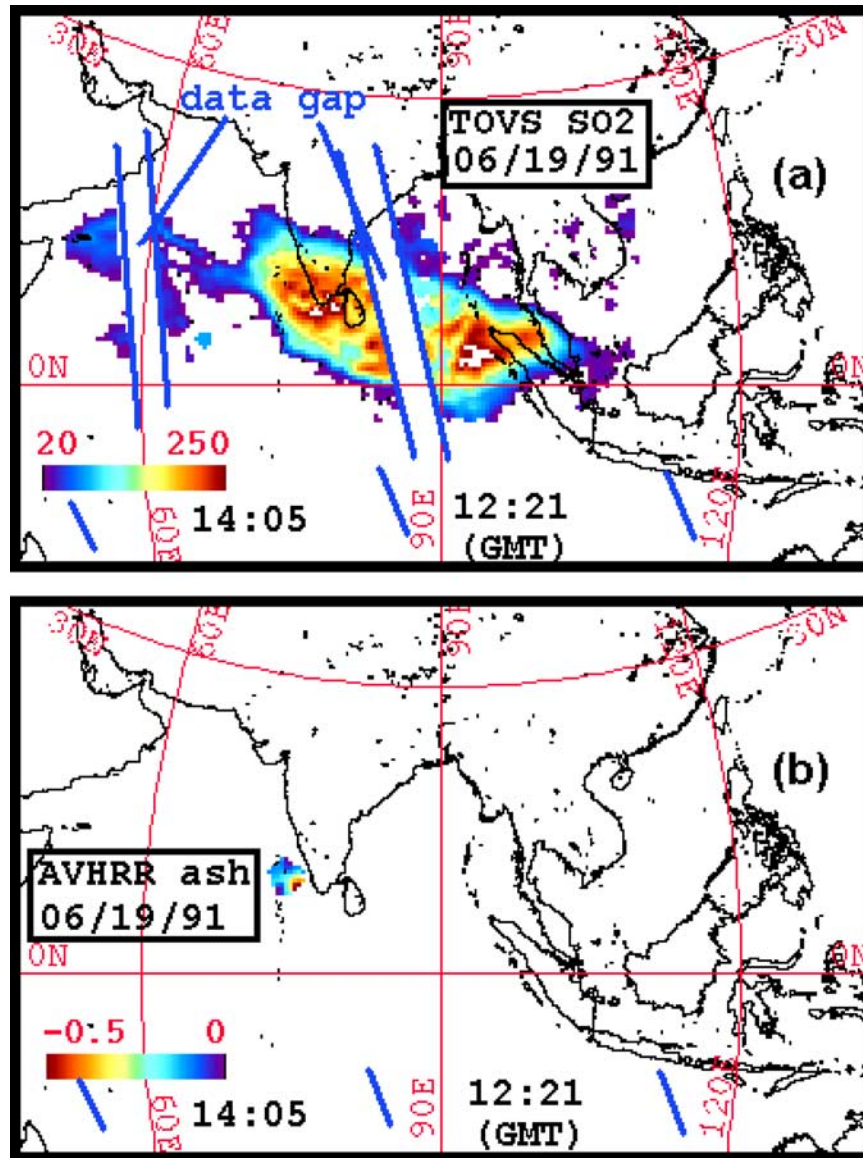


**Figure 21.** NOAA-12 maps: (a) TOVS SO<sub>2</sub> cloud map and (b) AVHRR BTD (ash cloud) map with atmospheric correction method applied. Latitude and longitude grid spacing is 30°. The SO<sub>2</sub> values are represented in Dobson Units (DU), and BTD values are represented in degrees Kelvin. The image sensing times are approximately the central pixel sensing time of the starting and ending orbits in GMT as indicated in the figures.

0.5  $\mu\text{m}$ ) particles are carried out using HIRS/2 data for up to 111 hours after eruption (Table 5). Figure 22 shows the 16 June 11:44 (GMT) burden maps of ash, ice, and sulfate from HIRS/2 multi-band retrievals. More sulfate remains to the east of the cloud while more ash is to the west of the cloud.

[22] Generally the HIRS/2 mass results for ash are 20–50% higher than AVHRR results for the first three days and then fall to values that are nearly the

same after 3 days (Figure 23 and Tables 3 and 5). The uncertainties for AVHRR and HIRS/2 retrievals are  $\pm 53\%$  [Wen and Rose, 1994; Gu *et al.*, 2003] and  $\pm 85\%$  [Yu and Rose, 2000], respectively, though the counteracting effects of ash and ice challenge the validation of AVHRR two band retrievals (the whole pixel is classified as either ash only or ice only in the AVHRR two-band retrieval). The ash masses estimated by AVHRR data are low because ash is counteracted by ice in part and because there are complexities

**Table 3.** Fine Ash (1–12  $\mu\text{m}$ ) Retrieval Results for Pinatubo Volcanic Clouds Using AVHRR<sup>a</sup>

Date	Time, GMT	Hours After Eruption	Ash Mass, Mt	Mean Effective Radius, $\mu\text{m}$	Mean Particle Radius, $\mu\text{m}$	Optical Depth (11 $\mu\text{m}$ )	Cloud Area ( $\times 10^6 \text{ km}^2$ )
6/15/91	06:30	0.82	25.75	9.56	3.20	2.65	0.665
	10:20&12:06	5.53	33.74	10.21	3.41	2.44	1.312
	17:58&19:41	13.14	33.98	9.50	3.18	1.82	2.042
6/16/91	07:16	25.58	20.44	7.90	2.64	1.48	3.880
	10:00&11:44	29.18	19.14	8.82	2.95	1.65	3.085
	20:05	38.40	15.20	8.38	2.80	1.32	3.535
6/17/91	07:19&09:00	50.48	10.05	9.59	3.21	1.56	3.267
	11:21&13:01	54.50	12.11	8.32	2.78	1.46	2.760
	19:16&29:59	66.94	6.91	8.67	2.90	1.45	1.649
6/18/91	05:51&07:25&08:43	73.60	2.71	8.43	2.82	1.12	0.780
	12:41&14:34&16:08	80.73	3.28	8.67	2.90	1.53	0.295
	20:47&22:22&23:59	88.70	3.72	9.48	3.17	1.30	0.246
6/19/91	08:38&10:20&12:04	100.67	1.58	8.30	2.78	1.22	0.137
	12:21&14:05&15:44	104.36	0.89	8.69	2.91	1.54	0.107

<sup>a</sup>Note: The image time is the central pixel sensing time if only one orbit involved or the central pixel sensing times of each individual orbit. Hours after eruption is based on the middle of the sensing time in column 2 and the starting time of the eruption is 05:41 (GMT), 15 June 1991.

in the retrieval caused by tropical clouds. The AVHRR results after 18 and 19 June are unreliable because the ash signal is very weak. The overall ash removal rates derived from both sensors are similar, and thus may be indicative of the real values.

[23] The total masses of fine ash from both HIRS/2 and AVHRR show decreasing trends with time while the mean effective radii remain almost constant (Figure 23 and Tables 3 and 5). The HIRS/2 values for ash are probably more accurate because they incorporate and measure the influence of ice. As the data are timed with respect to the start of the eruption, the first three points are within

the eruption period with an increasing trend (Figure 23). About 92% of the fine ash (1–12  $\mu\text{m}$ ) detected by AVHRR and 89% of the fine ash (1–15  $\mu\text{m}$ ) detected by HIRS/2 were removed from stratosphere 73 hours after eruption (about three days) and about 99% of the detected fine ash was removed from the atmosphere 110 hours after eruption (Tables 3 and 5). The volcanic ash cloud areas for both HIRS/2 and AVHRR retrievals increased for the first 24 hours after eruption, and then decreased dramatically to 20% of its maximum in 70 hours and to 5% of its maximum after 94 hours, during a period when the  $\text{SO}_2$  cloud area continuously increased (Figure 24 and Tables 3 and 5). The ash cloud areas based on HIRS/2

**Table 4.** Parameters Used in AVHRR Ash Retrieval (Table 3) With Atmospheric Correction

Date and Time, GMT	Band 4 Temperature of Underlying Surface, K	Band 5 Temperature of Underlying Surface, K	Cloud Temperature, K	BTD Value, K
6/15/91 06:30	285	283	200	<2.0
6/15/91 10:26&12:06	285	283	190	<2.0
6/15/91 17:58&19:41	285	282	200	<2.0
6/16/91 07:26	288	285	200	<1.0
6/16/91 10:00&11:44	285	282	200	<1.0
6/16/91 20:05	285	282	200	<0.5
6/17/91 07:19&09:00	290	288	200	<0.5
6/17/91 11:21&13:01	293	290	190	<0.5
6/17/91 19:16&20:59	285	282	190	<1.0
6/18/91 05:51&07:25&08:43	295	293	200	<0.5
6/18/91 12:41&14:34&16:08	288	285	200	<0.5
6/18/91 20:47&22:22&23:59	290	288	200	<0.5
6/19/91 08:38&10:20&12:04	288	285	200	<0.0
6/19/91 12:21&14:05&15:44	293	290	200	<0.0

**Table 5.** Fine Ash (1–15  $\mu\text{m}$ ), Fine Ice (1–30  $\mu\text{m}$ ), and Sulfate (0.1–0.5  $\mu\text{m}$ ) Retrieval Results for Pinatubo Volcanic Clouds Using HIRS/2 Data<sup>a</sup>

Date	Time, GMT	Hours After Eruption	Ash Mass, Mt	Ash Effective Radius, $\mu\text{m}$	Optical Depth, $\mu\text{m}$	Ice Mass, Mt	Ice Effective Radius, $\mu\text{m}$	Sulfate Mass, Mt	Sulfate Effective Radius, $\mu\text{m}$	Ash Cloud Area ( $\times 10^6 \text{ km}^2$ )
6/15/91	06:30	0.82	30.85	8.62	1.31	46.03	23.37	3.33	0.15	0.739
	10:26	4.75	37.61	8.36	1.51	62.47	25.54	3.52	0.16	1.045
	10:53	5.2	48.57	8.55	1.53	80.95	23.75	2.38	0.21	1.537
	18:07	11.58	45.55	8.28	1.64	84.44	24.77	3.52	0.20	2.329
6/16/91	00:52	19.18	37.47	8.90	1.15	52.01	23.75	8.07	0.15	3.512
	01:18	19.62	41.94	8.97	1.45	59.75	23.94	7.22	0.14	2.923
	07:28	25.78	28.35	7.66	1.30	40.32	27.47	6.67	0.14	4.071
	11:44	30.05	38.24	7.31	1.69	46.53	24.50	5.81	0.16	3.719
	12:20	30.65	26.59	6.84	1.12	49.48	26.73	9.57	0.15	3.595
	20:05	38.4	30.54	9.33	1.01	42.84	26.02	6.30	0.14	4.019
	6/17/91	00:12–00:33	42.69	37.00	7.55	1.38	32.93	27.74	8.66	0.16
	00:39–02:01	43.65	18.66	7.31	0.94	35.27	25.93	7.77	0.13	3.511
	07:25–08:43	50.38	27.70	8.30	1.01	39.86	26.16	7.24	0.14	3.618
	11:39–13:05	54.68	18.44	7.21	1.46	21.65	26.12	13.07	0.16	2.714
	12:07–13:31	55.13	17.72	7.53	1.21	29.25	28.44	6.82	0.13	2.285
	19:16–20:59	62.44	20.94	7.23	1.04	32.59	25.52	10.61	0.14	2.013
6/18/91	01:55–04:58	69.76	10.32	8.13	0.74	18.03	27.27	10.41	0.16	1.756
	02:21–05:25	70.2	5.53	7.22	0.73	9.99	28.28	6.22	0.14	1.016
	07:25–08:43	74.38	6.48	8.12	0.95	12.02	26.64	7.03	0.13	0.812
	12:41–16:08	80.73	5.38	6.32	1.15	12.98	26.28	10.6	0.16	0.974
	12:53–16:05	80.8	2.94	6.26	1.13	7.14	26.41	8.97	0.14	0.513
	20:47–21:22	87.39	3.22	6.77	1.04	8.88	27.11	7.44	0.13	0.336
	6/19/91	01:58–03:41	93.14	2.90	7.83	1.58	4.58	25.35	11.28	0.15
	02:20–05:25	94.19	2.27	7.84	1.24	5.53	25.38	14.63	0.13	0.271
	07:25–08:43	98.38	2.73	6.20	1.12	6.00	27.32	9.94	0.14	0.196
	12:41–16:08	104.73	1.20	7.58	0.88	4.30	28.29	13.2	0.15	0.151
	12:53–16:05	104.8	1.85	7.74	0.82	3.00	27.49	16.16	0.13	0.135
	20:47–21:22	111.39	0.49	6.64	0.99	2.72	29.18	12.06	0.14	0.095

<sup>a</sup>Note: The image time is either the central pixel sensing time if only one orbit involved or the central pixel sensing times of the starting and ending orbits if more than one orbit involved. Hours after eruption is based on the middle of the sensing times in column 2 and the eruption starting time is 05:42 (GMT), 15 June 1991.

retrieval are 20–30% larger than those detected by AVHRR 10–55 hours after eruption (Figure 24). These differences reflect the significant amount of ice interference to the AVHRR split-window detection (Figure 25).

[24] On the basis of dense rock equivalent volume of 3.7–5.3  $\text{km}^3$  [Scott *et al.*, 1996] and a dacitic magma density of 2.4  $\text{g/cm}^3$  [Scott *et al.*, 1996], 8880–12720 Mt of ash were erupted from Pinatubo on 15 June 1991. Therefore the fine ash mass detected by the satellite is 0.6–0.9% of the total ash mass, similar to the proportions determined by Schneider *et al.* [1999] for the 1982 El Chichón eruption. Most of the mass of erupted ash falls out quickly because it is coarser than 100  $\mu\text{m}$  in diameter and is not seen by the satellite. The retrieved mean effective radii from both AVHRR

model and HIRS/2 model are comparable to the monomodal peak (11  $\mu\text{m}$  in radius) found in distal deposits collected further than 45 km from the vent by Darteville *et al.* [2002].

#### 4.4. Ice Retrievals Using the AVHRR Split-Window and HIRS/2 Multibands

[25] Ice (1–30  $\mu\text{m}$  in radius) properties were retrieved using the refractive index and density of ice using AVHRR data and following the work of Rose *et al.* [1995] (Table 6). Higher masses (2–3 times) of ice than ash were detected in the Pinatubo cloud and the ice masses decreased rapidly, at rates that mimic the removal rates of ash (Figure 25). The multiband HIRS/2 ice results shown in Table 5 and Figure 25, like the ash results, are probably more accurate than AVHRR

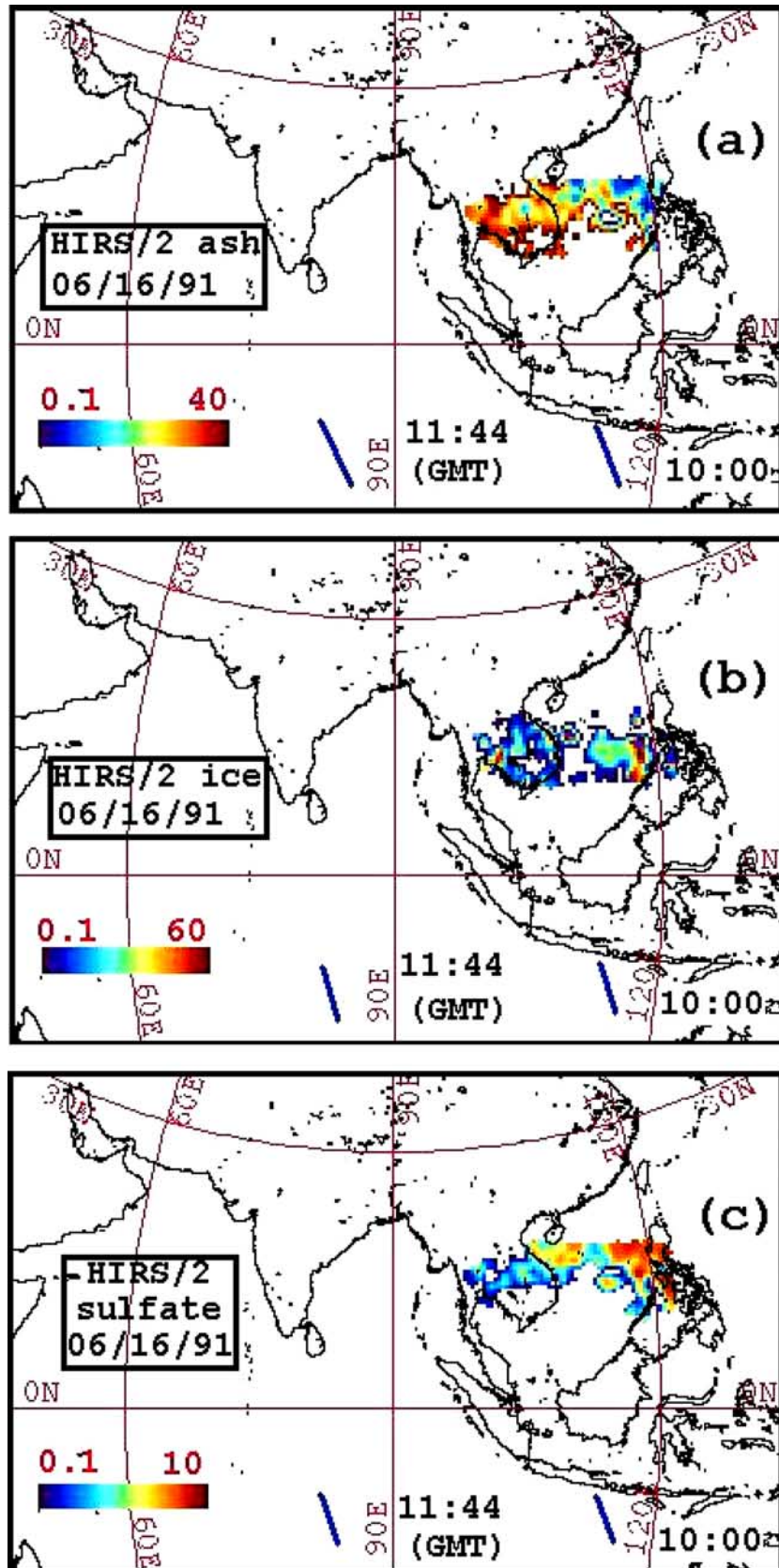
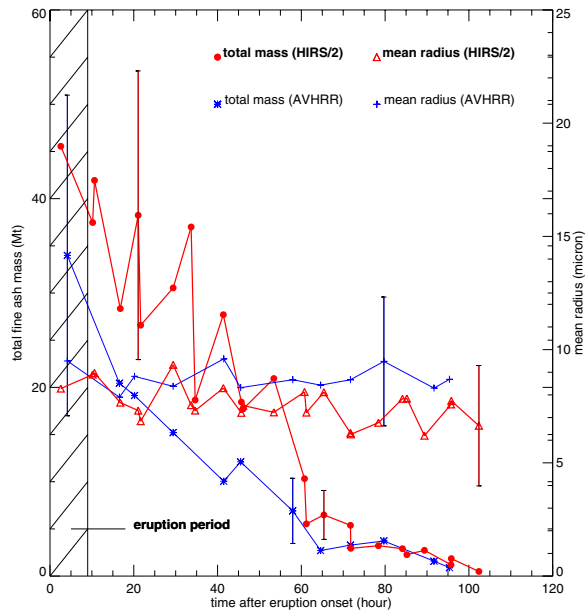


Figure 22



**Figure 23.** Fine ash mass and mean effective radius of the 1991 Pinatubo volcanic ash cloud as a function of time, using AVHRR split-window retrieval (ash particle size 1–12  $\mu\text{m}$ ) (Table 3) and HIRS/2 retrieval (particle size 1–15  $\mu\text{m}$ ) (Table 5). The ash masses decrease with time, while the mean effective radius remains almost constant. The error bars show the error range of the data (proportional to the total) at a few specific points (see text for discussion).

results as the coexisting ice, ash, sulfate particles are retrieved simultaneously.

[26] The HIRS/2 mass results for ice are generally higher than AVHRR results most of time, especially during the first three days (Figure 25 and Tables 5 and 6). As with ash retrievals, the ice masses estimated by AVHRR data are inaccurate because ice is counteracted by ash in part and because there are complexities in the retrieval caused by tropical clouds. The ice masses from both HIRS/2 and AVHRR show decreasing trends over time while the mean effective radii remain almost constant (Figure 25 and Tables 5 and 6). Note that the first three points are within the eruption period, and display an increasing trend

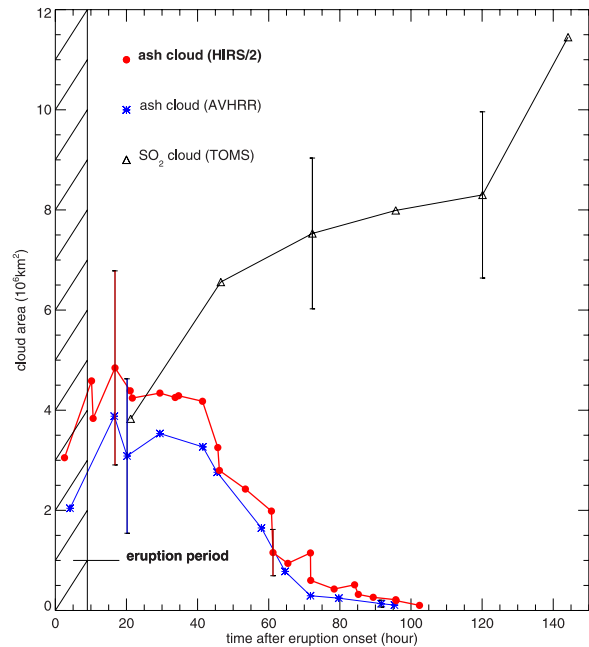


**Figure 24.** The 1991 Pinatubo volcanic ash cloud area as a function of time based on AVHRR data (Table 3) and HIRS/2 data (Table 5). The Pinatubo  $\text{SO}_2$  cloud area as a function of time based on TOMS data [Guo *et al.*, 2004]. The ash cloud area increases for up to  $\sim 25$  hours after the start of the main eruption and then decreases dramatically with time. The  $\text{SO}_2$  cloud area increases continuously over time. The error bars indicate the error range of the data at a few specific points (see text for discussion).

(Figure 25). About 90% of the ice detected by AVHRR and HIRS/2 was removed from the stratosphere 73 hours after eruption (three days), and about 98% of the detected ice was removed in 110 hours (Tables 5 and 6). The pattern of decrease of both ice and ash was similar.

#### 4.5. Sulfate Retrievals Using the Multiband HIRS/2 Data

[27] HIRS/2 also includes retrieval data on sulfate particles in the Pinatubo cloud (Table 5). The total mass of sulfate increases with time while the mean effective radius remains almost constant ( $0.14\text{--}0.20 \pm 0.12 \mu\text{m}$ ) (Figure 26 and Table 5). The

**Figure 22.** HIRS/2 maps: (a) ash burden, (b) ice burden, and (c) sulfate burden. Latitude and longitude grid spacing is  $30^\circ$ . The burdens are represented in  $\text{Kt}/\text{km}^3$ . The image sensing times are approximately the central pixel sensing time of the starting and ending orbits in GMT as indicated in the figures. Note the different scales used: the burdens of sulfate are much less than those of ash or ice.

**Table 6.** Ice (1–30  $\mu\text{m}$ ) Retrieval Results for Pinatubo Volcanic Clouds Using AVHRR Data<sup>a</sup>

Date	Time, GMT	Hours After Eruption	Ice Mass, Mt	Mean Effective Radius, $\mu\text{m}$	Mean Particle Radius, $\mu\text{m}$	Optical Depth (11 $\mu\text{m}$ )
6/15/91	06:30	0.82	44.76	20.01	6.69	2.23
	10:20&12:06	5.53	59.91	22.39	7.49	3.84
	17:58&19:41	13.14	60.76	26.09	8.73	2.36
6/16/91	07:16	25.58	43.54	26.89	9.00	1.83
	10:00&11:44	29.18	28.34	25.44	8.51	1.67
	20:05	38.40	29.49	29.02	9.71	1.48
6/17/91	07:19&09:00	50.48	15.86	29.97	10.03	1.59
	11:21&13:01	54.50	21.88	29.86	9.99	1.47
	19:16&29:59	66.94	14.90	27.87	9.32	1.94
6/18/91	05:51&07:25&08:43	73.60	4.78	29.06	9.72	1.14
	12:41&14:34&16:08	80.73	5.97	29.77	9.96	1.64
	20:47&22:22&23:59	88.70	5.83	29.99	10.03	1.30
6/19/91	08:38&10:20&12:04	100.67	2.88	30.00	10.03	1.23
	12:21&14:05&15:44	104.36	1.58	30.00	10.03	1.59

<sup>a</sup>Note: The image time is the central pixel sensing time if only one orbit involved or the central pixel sensing times of each individual orbit connected by &. Hours after eruption is based on the middle of the sensing times in column 2 and the beginning time of the eruption is 05:41 (GMT), 15 June 1991.

retrieved sulfate effective radii are similar to the maximum pure sulfate aerosol radius (0.2  $\mu\text{m}$  [Turco *et al.*, 1983]) and the effective radii of the Pinatubo sulfate aerosols (0.1–0.2  $\mu\text{m}$ ) just after eruption by Russell *et al.* [1996]. About 12–15 Mt sulfate was detected within the Pinatubo cloud 110 hours after the eruption (Figure 26). The sulfate mass retrieved is significant ( $\sim 4$  Mt) within an hour after eruption (exponential curve, Figure 26), although the first four retrievals (Table 5) are likely less reliable than later measurements owing to high optical depths.

#### 4.6. Analysis of Cloud Movements

[28] Holasek *et al.* [1996] reported the maximum Pinatubo plume height could be as high as  $\sim 39$  km, and the cloud heights were estimated at 20–25 km after 14 hours using cloud shadow and thermal methods. Self *et al.* [1996] report the maximum plume height could be  $>35$  km and the plume heights are 23–28 km after 15–16 hours using temperature measurements. Read *et al.* [1993] estimated that the peak  $\text{SO}_2$  layer was at 26 km using data from the Microwave Limb Sounder (MLS) experiment on the Upper Atmosphere Research Satellite (UARS). The neutral buoyant regions of the Pinatubo aerosol were also estimated by other measurements: 17–26 km (lidar) by

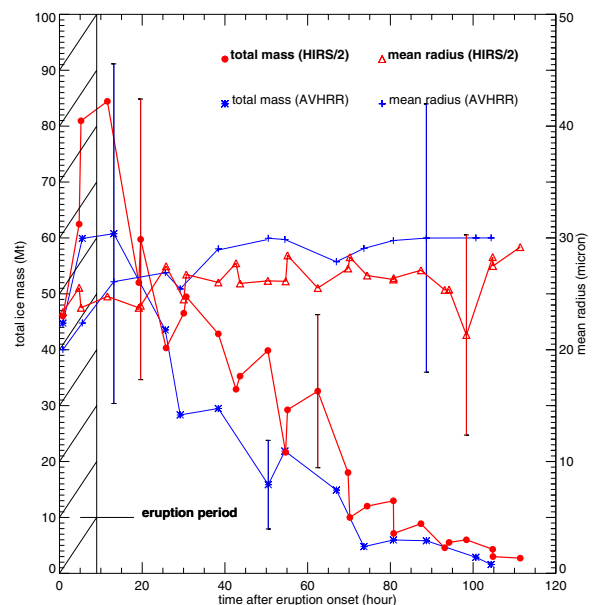


**Figure 25.** Total ice (1–30  $\mu\text{m}$ ) mass and mean effective radius of the 1991 Pinatubo volcanic ash cloud as a function of time, using AVHRR split-window retrieval (Table 6) and HIRS/2 retrieval (Table 5). The total ice masses decrease with time, while the mean effective radius remains almost constant. Ice masses are 179% to 213% of the ash masses shown in Figure 23 except for one point. The error bars indicate the error range of the data at a few specific points (see text for discussion).

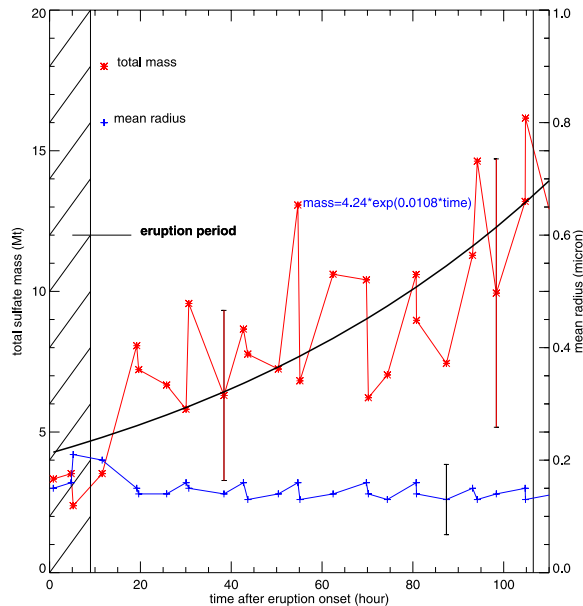


**Figure 26.** Total fine sulfate (0.1–0.5  $\mu\text{m}$ ) mass and mean effective radius of the 1991 Pinatubo volcanic ash cloud as a function of time, measuring using HIRS/2 data (Table 5). The total fine sulfate masses increase with time, while the mean effective radius remains almost constant. The error bars indicate the error range of the data at a few specific points (see text for discussion).

*DeFoor et al.* [1992], 20–23 km (balloon) by *Deshler et al.* [1992], 17–28 km (lidar) by *Jaeger* [1992], and 17–25 km (lidar) by *Avdyushin et al.* [1993].

[29] To help reconcile cloud positions to atmospheric conditions, forward isentropical wind trajectory simulations (NASA Goddard Space Flight Center) were run using Pinatubo’s eruption start time. The overall movements of Pinatubo  $\text{SO}_2$  and ash clouds match the 25 km and 22 km wind trajectories quite well, except during the first 15 hours (Table 7), meaning the central parts of the  $\text{SO}_2$  and ash clouds were 25 km and 22 km, respectively. The wind directions are easterly at all levels above the tropopause and the wind intensity increases slightly with altitude. Thus cloud heights can easily be determined as the higher air parcels travel longer distances. The inaccuracy for the wind trajectory results in the first 15 hours after eruption is due to the interference from the Typhoon Yunya as no real-time atmospheric profiles were measured during the eruption periods and the atmospheric profiles

**Table 7.** Distances and Directions of Pinatubo Volcanic  $\text{SO}_2$  and Ash Cloud Leading Edges and NASA GSFC Wind Trajectory Results at 22 km and 25 km<sup>a</sup>

Hours After Eruption <sup>b</sup>	SO <sub>2</sub> Cloud Leading Edges		Ash Cloud Leading Edges		Wind Trajectory (25 km)		Wind Trajectory (22 km)	
	Distance, km	Direction, degree <sup>c</sup>	Distance, km	Direction, degree	Distance, km	Direction, degree	Distance, km	Direction, degree
0.82	1477.7 <sup>d</sup>	286.2 <sup>d</sup>	102.2 <sup>d</sup>	296.0 <sup>d</sup>	455.7	268.6	274.2	267.8
5.53	1555.3 <sup>d</sup>	273.4 <sup>d</sup>	998.2 <sup>d</sup>	295.3 <sup>d</sup>	919.8	270.1	625.4	270.0
13.14	1548.9 <sup>d</sup>	269.5 <sup>d</sup>	1288.9 <sup>d</sup>	279.0 <sup>d</sup>	1620.2	267.9	1199.8	268.1
22.04	2100.2	266.7	1446.4	282.0	1872.0	267.7	1232.2	267.5
25.58	3124.8	270.0	1842.8	273.1	2191.0	267.7	1325.7	267.1
29.18	3252.6	269.8	2107.0	271.6	2690.6	268.7	1650.3	267.5
38.40	3603.1	269.6	2551.4	269.8	3222.0	267.1	2018.1	268.7
50.48	3679.1	270.6	2913.0	269.5	3443.7	266.7	2685.8	269.5
54.50	3847.1	269.3	2696.0	270.8	3728.0	267.0	2932.8	270.3
66.94	5172.2	270.2	3020.2	267.7	4302.7	268.3	3308.3	269.3
73.60	5587.5	269.9	3681.0	273.5	5074.4	269.3	3763.9	268.8
80.73	5690.6	268.9	3820.5	274.7	5486.2	269.3	3827.2	270.0
88.70	6125.2	269.2	4278.2	277.2	5986.1	269.7	4184.7	270.7
100.67	7063.4	269.6	4974.7	275.0	6819.8	270.0	4924.5	273.0
104.36	7254.0	269.1	5226.6	274.5	7381.8	270.1	5211.6	272.3

<sup>a</sup> All distances and directions are measured relative to Pinatubo volcano (15.13N, 120.35E).

<sup>b</sup> One TOMS AI (16 June) and 14 AVHRR ash maps are used in the calculation; the ending times in the first column of the table correspond to image sensing times.

<sup>c</sup> Direction is labeled the same as wind direction; 0 degree indicates north direction and clockwise increase.

<sup>d</sup> Mass weighted latitude and longitude locations are used instead of cloud leading edge locations due to opaque cloud area and clouds from precursive activities.

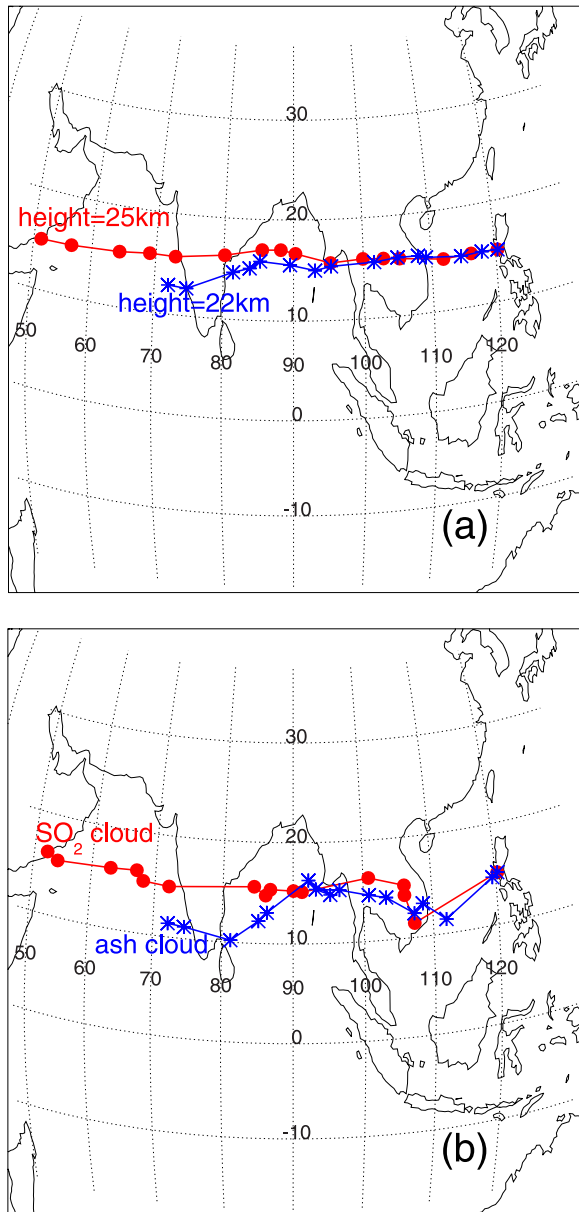


**Figure 27.** (a) Five days of NASA GSFC isentropic wind forward trajectory results (22 and 25 km levels) starting from 15 June 91 with each point representing one image sensing time. (b) Leading edge SO<sub>2</sub> and gas cloud locations with each point.

used in trajectory calculations are interpolated from the measured profiles several hundred miles away, possibly minimizing the influence of the typhoon. The movement of the ash cloud over the Bay of Bengal between Thailand and India also does not match the trajectory results precisely (Table 7 and Figure 27). The effects of a tropical thunderstorm there may account for this slight

deviation. The SO<sub>2</sub> cloud moved about 7300 km west and the ash cloud moved about 5200 km west 104 hours after eruption (Table 7). The locations of forward trajectory results at each sensing time (Figure 27a) match the leading edge cloud positions for each image at 22 km for ash and 25 km for SO<sub>2</sub> (Figure 27b).

## 5. Summary of Main Results

[30] 1. Ice masses several times greater than ash masses were present in the Pinatubo volcanic cloud. These make accurate particle retrievals possible only with multispectral infrared data, such as HIRS/2 and MODIS (of course MODIS did not exist then).

[31] 2. Although it is difficult to locate the ash cloud precisely, a slight vertical separation of the SO<sub>2</sub>-rich volcanic cloud (~25 km high) and ash-rich volcanic cloud (~22 km high) is consistent with the apparently slightly faster westward migration of SO<sub>2</sub> anomalies compared to ash. Lack

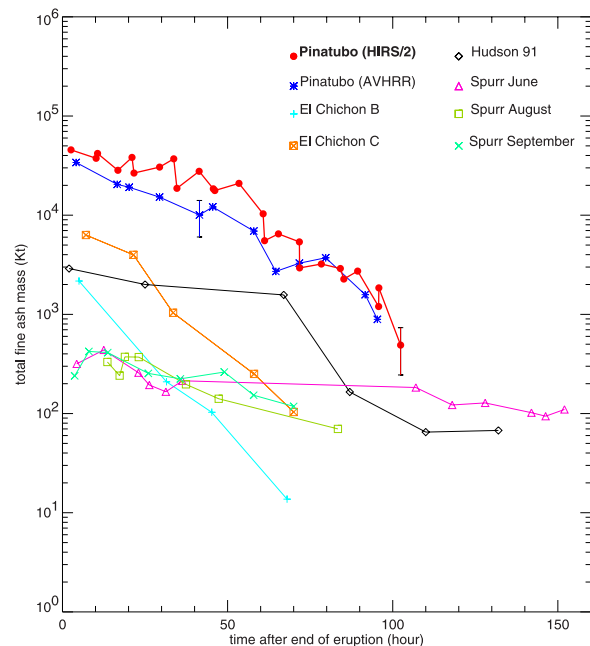


**Figure 28.** Total ash mass of volcanic ash clouds of the 1991 Pinatubo (Tables 3 and 5), the 1982 El Chichón [Schneider *et al.*, 1999], the 1991 Hudson [Constantine *et al.*, 2000], and the 1992 Spurr [Rose *et al.*, 2001]. All of them decrease with time (see text for discussion). The error bars indicate the error range of the data at a few specific points (see text for discussion).

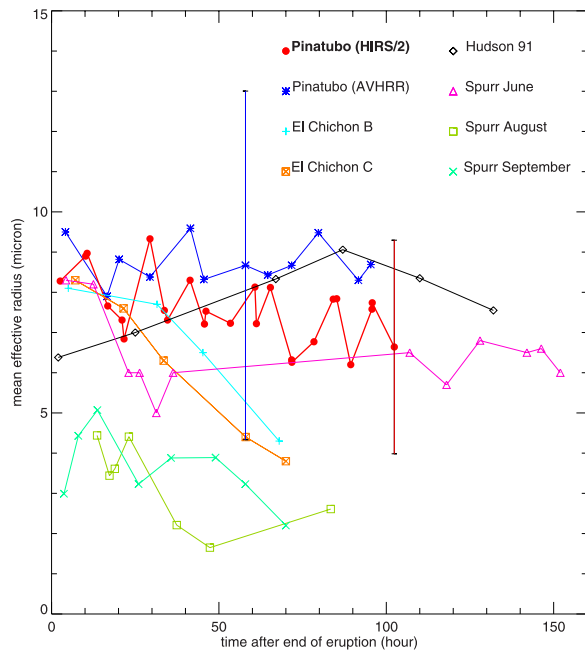


**Figure 29.** Mean effective radius of volcanic ash clouds of the 1991 Pinatubo (Tables 3 and 5), the 1982 El Chichón [Schneider et al., 1999], the 1991 Hudson [Constantine et al., 2000], and the 1992 Spurr [Rose et al., 2001] (see text for discussion). The error bars indicate the error range of the data at a few specific points (see text for discussion).

of windshear may have made detection of separation more difficult.

[32] 3. Both ash and ice decreased rapidly to a small percentage (~10%) of their peak masses after 3 days of atmospheric residence in the volcanic cloud.

[33] 4. Sulfate particle masses in the Pinatubo clouds, retrieved using multispectral IR sensing, increased by 2–3 times (to 12–15 Mt) during the first 111 (five days) after eruption.

## 6. Discussion

### 6.1. How Much Ice is Too Much for Accurate Two Band Retrievals?

[34] In the past, the two band IR split-window retrievals on AVHRR, GOES, and MODIS have been used for ash particle retrievals for many eruptions. The Pinatubo case demonstrates that ice can severely affect such retrievals and necessitates a multispectral retrieval using HIRS/2 or MODIS data if ice is abundant enough. Although it is a non-marine volcano, Pinatubo’s environmental variables were especially favorable for ice, because of the moist tropical location and low elevation. This example shows that when ice masses and ash masses are similar in magnitude in volcanic clouds, two-band retrievals are adversely affected.

[35] If two-band retrievals are done on a volcanic cloud which also contains ice, the mass estimates will be lower than the true values and the effective radius values are also likely to be larger. We need to develop ways to know when ice contents are significant from the satellite data alone (see Figures 3 and 4). One distinctive feature of the Pinatubo cloud is that even though it is very large and has very cold stratospheric temperatures and a very large temperature contrast with the warm

**Table 8.** Ash and Ice Removal Rates From Different Eruptions, Estimated With Remote Sensing

Volcano	Period of Measurement (Hours After the End of Eruption)	Particle Type	Mean Removal Rate, Kt/hr	e-Folding Time, hours	Reference
1991 Pinatubo (HIRS/2)	4.1–95.4	ash	482	24	this paper
1991 Pinatubo (HIRS/2)	2.6–102.4	ice	819	30	this paper
1991 Pinatubo (AVHRR)	4.1–95.4	ash	363	27	this paper
1991 Pinatubo (AVHRR)	4.1–95.4	ice	648	27	this paper
1982 El Chichón B	5.0–68.0	ash	34.2	13	Schneider et al. [1999]
1982 El Chichón C	7.1–70	ash	98.7	15	Schneider et al. [1999]
1991 Hudson	2.0–132.0	ash	21.8	30	Constantine et al. [2000]
June 1992 Spurr	12.5–152.0	ash	2.35	143	Rose et al. [2001]
August 1992 Spurr	13.6–83.4	ash	3.74	43	Rose et al. [2001]
September 1992 Spurr	8.0–70.0	ash	4.92	52	Rose et al. [2001]
2000 Hekla	6.2–23.9	ice	48	8	Rose et al. [2003]

**Table 9.** TOMS AI Values of the Pinatubo Volcanic Clouds the First Week After Eruption<sup>a</sup>

Date	Time, GMT	AI (Max Value)	AI (Min Value)
6/15/91	03:26	7.5	-0.1
6/16/91	2:01–3:44	7.5	-0.3
6/17/91	2:40–5:45	7.0	-1.3
6/18/91	4:14–7:42	2.5	-1.0
6/19/91	3:02–7:45	1.5	-1.0
6/20/91	3:38–7:57	2.2	-0.8
6/21/91	3:26–8:15	1.7	-1.0

<sup>a</sup>Note: The whole volcanic cloud areas were accounted except when the volcanic cloud was overlapped by dust storm or sand storm in the regions of Middle East and Africa.

surface below, the brightness temperature differences are quite moderate and are rarely more than a few degrees. We think this is due to the effects of ice and possibly other components of the volcanic cloud, and at least in the first two days, there could be high dense meteorological clouds that suppress the temperature contrasts.

## 6.2. Does Ice Enhance The Ash Fallout?

[36] *Rose et al.* [1995] first pointed out the important role of ice in the ash-removal process, and that ice-rich volcanic ash clouds may have a shorter atmospheric residence time. Large amounts of different kinds of hydrometeors (ice, rain, hail, snow, sleet, etc.), especially ice, exist in some volcanic clouds, such as the 1994 Rabaul cloud [*Rose et al.*, 1995], the 26 December 1997 Montserrat cloud [*Mayberry et al.*, 2002], and the 2000 Hekla cloud [*Rose et al.*, 2003]. One of the principal roles of ice in the volcanic cloud is to form ice-ash aggregates and thus accelerate the ash fallout, as suggested by ATHAM simulation results [*Herzog et al.*, 1998; *Textor*, 1999] and described by *Rose et al.* [2000]. Different particle fallout velocities due to the different particle sizes can cause gravitational collision, where large particles collect smaller ones. Turbulent motions of ash particles may increase the likelihood of collision (R. Shaw, personal communication, 2003). The collisions result in particle aggregates if binding forces between the particles are strong enough. Moist particles have stronger short-range surface tension forces than dry particles [*Sparks et al.*, 1997]. Therefore volcanic clouds containing

higher H<sub>2</sub>O content can expect to have a greatly enhanced aggregation process. Fine ash particles can also serve as active cloud nuclei to enhance ice-ash aggregation as supported by ATHAM simulation [*Herzog et al.*, 1998] and ice can grow on ash nuclei as described by *Rose et al.* [2003]. The ash aggregates usually have a higher surface area relative to their masses and can be rapidly filled up with ice by deposition of water vapor and heterogeneous nucleation on the aggregates [*Wallace and Hobbs*, 1997]. Because of the abundant ice in the early Pinatubo volcanic cloud suggested by our data analysis, there should be water vapor from sublimation in the volcanic cloud. We do not measure this nor do we adequately consider the effects of this on our results. The importance of this may extend to other issues also, as water vapor should influence SO<sub>2</sub> oxidation to sulfate and could cause interference with SO<sub>2</sub> measurement using the IR (TOVS) sensor.

[37] Figures 28 and 29 compare the retrieved fine ash masses and mean effective radii for various eruptions. Table 8 compares remote sensing data which summarize the removal rates of ash particles from various volcanic clouds. We note the following in this table: (1) the e-folding times for ash (24–27 hours) and ice (27–30 hours) at Pinatubo are similar; (2) the e-folding times for the 1991 Hudson (21 hours), the 1982 El Chichón (13–15 hours), and the 2000 Hekla (8 hours) eruptions are shorter, indicating faster ash removal, while the three 1992 Spurr eruptions have much longer e-folding times (40–140 hours), indicating slower ash fallout. We need more data to see how these data can be fully explained, and no simple explanation emerges for the differences.

[38] The difference between e-folding times for SO<sub>2</sub> (25 days) and for ash (24–27 hours) is striking, however. The similarity of removal rates for ice and ash make it hard to imagine that ash and ice were removed separately without aggregation. *Darteville et al.* [2002] found one of the size peaks of the fallen ash particles within 45 km of the vent was 5.5 μm in radius. This is far too small to be explained by simple fallout mechanism, and likely

reflects aggregation. *Wiesner et al.* [2004] also pointed out that only aggregation could explain the fine-grained particles from the coast of Luzon up to South China Sea, as the high-velocity easterly wind at upper-troposphere and stratosphere would have transported fine-grained particles far beyond South China Sea without aggregation.

### 6.3. Does the Increase in Sulfate Match SO<sub>2</sub> Decrease Within the Whole Cloud?

[39] The sulfate mass retrieved is significant (4 Mt) even within one hour after eruption (Table 5, Figure 26). The observation of early sulfate based on HIRS/2 data was also noted for the 1982 El Chichón eruption by *Yu and Rose* [2000], and suggests that sulfate formation may be catalyzed in eruption columns. The mass of sulfate particles increases steadily for the 4 day period of analysis, producing 8–10 Mt additional sulfate mass. This rate of increase can be compared to the SO<sub>2</sub> decrease determined by *Guo et al.* [2004] of about 4–8 Mt for the same time period. Given the mass differences of sulfate and SO<sub>2</sub>, the two rates are within 50% which suggests that conversion of SO<sub>2</sub> to sulfate is the main cause of sulfate increases seen.

[40] Non-absorbing aerosols, such as sulfate, can produce negative AI signals [*Seftor et al.*, 1997]. Negative TOMS AI signals existed on the Pinatubo AI maps the first week after eruption (later the SO<sub>2</sub> cloud overlapped with dust storms and sandstorms in the Middle East and Africa, making the negative AI signals difficult to identify). The negative AI signals were very weak (usually between –1 and 0) (Table 9). The relatively weak sulfate signal might be due to the larger particle sizes (0.15–0.20 μm), because only particles smaller than 0.05 μm can produce strongly negative AI values [*Rose et al.*, 2003].

## 7. Conclusions

[41] We mapped the 2-D distribution of Pinatubo ash clouds using two-band AVHRR ash maps and TOMS AI maps. The cloud expanded for about 24 hours and had a maximum area of about  $5 \times 10^6$  km<sup>2</sup> and then decreased quickly to less than  $1 \times 10^6$  km<sup>2</sup> after about 3 days. Comparison of these

maps with SO<sub>2</sub> maps from TOMS and TOVS offer little evidence that SO<sub>2</sub>-rich and ash-rich portions of the Pinatubo volcanic cloud separated, though the SO<sub>2</sub> cloud may be traveling to the west slightly faster than the ash cloud. A slight vertical separation of SO<sub>2</sub>-rich (~25 km high) and ash-rich (~22 km high) volcanic clouds is consistent with the slight faster migration of SO<sub>2</sub> than ash westerly, though uncertainty exists due to the difficulty in precisely locating the ash cloud.

[42] The abundance of ice in the Pinatubo volcanic clouds complicates the ash and ice retrieval results by AVHRR two-band split-window method because of the contrary effects of ash and ice and because of complexities caused by tropical clouds. Multiband retrieval of ash, ice, and sulfate properties using HIRS/2 data is probably more indicative of what really happened in this volcanic cloud.

[43] The multispectral remote sensing possible from HIRS/2 [*Yu and Rose*, 2000] allows for a more realistic sensing of particles in the case of Pinatubo, where both ice and ash are abundant. It also allows for retrieval of particle size, optical depth, and masses of three different particle compositions (ash, ice, and sulfate). The ice and ash masses in the Pinatubo cloud were about 80 Mt (8–16% of total magmatic H<sub>2</sub>O) and 50 Mt (0.6–0.9% of total erupted ash) maximum, and declined rapidly to less than 10% of their maximum within 3 days. We speculate that ash surfaces were enhancing ice formation and that fallout was also enhanced. The e-folding removal times estimated for Pinatubo ice and ash were about 24–30 hours which contrasts strikingly with comparable SO<sub>2</sub> e-folding (25 days).

[44] Sulfate particles were present in the Pinatubo cloud even very soon after eruption and the masses of sulfate increased during the first four days at a rate consistent with the SO<sub>2</sub> decreases. Initially detected sulfate mass was 3.3 Mt and then after 5 days was 12–16 Mt.

## Acknowledgments

[45] Song Guo acknowledges support from the U.S. National Science Foundation (NSF EAR 01-06875) and a NASA Graduate Student Fellowship. We acknowledge the help of

Leslie R. Lait at NASA Goddard Space Flight Center for the use of a NASA wind trajectory model. We also thank A. J. Prata from CSIRO in Australia for providing the raw TOVS SO<sub>2</sub> retrieval codes. We also benefited from comments by A. J. Prata, Hans Graf, Steven Self, and an anonymous reviewer.

## References

- Avdyushin, S. I., G. F. Tulinov, M. S. Ivanov, B. N. Kuzmenko, I. R. Mezhuev, B. Nardi, A. Hauchecorne, and M. L. Chanin (1993), Spatial and temporal evolution of the optical thickness of the Pinatubo aerosol cloud in the northern hemisphere from a network of ship-borne and stationary lidars, *Geophys. Res. Lett.*, *20*, 1963–1966.
- Berk, A., S. Bernstein, and D. C. Robertson (1989), MODTRAN: A moderate resolution model for LOWTRAN 7, *AFGL-TR-89-0122*, U.S. Air Force Geophys. Lab., Hanscom Air Force Base, Mass.
- Bernard, A., U. Knittel, B. Weber, D. Weis, A. Albrecht, K. Hattori, J. Klein, and D. Oles (1996), Petrology and geochemistry of the 1991 eruption products of Mount Pinatubo, in *Fire and Mud: Eruptions and Lahars of Mount Pinatubo, Philippines*, edited by C. G. Newhall and R. S. Punongbayan, pp. 767–797, Philippine Inst. of Volcanol. and Seismol., Quezon City.
- Bluth, G. J. S., T. J. Casadevall, C. C. Schnetzler, S. D. Doiron, L. S. Walter, A. J. Krueger, and M. Badruddin (1994), Evaluation of sulfur dioxide emissions from explosive volcanism: The 1982–1983 eruptions of Galunggung, Java, Indonesia:, *J. Volcanol. Geotherm. Res.*, *63*, 243–256.
- Constantine, E. K., G. J. S. Bluth, and W. I. Rose (2000), TOMS and AVHRR sensors applied to drifting volcanic clouds from the August 1991 eruptions of Cerro Hudson, in *Remote Sensing of Active Volcanism*, *Geophys. Monogr. Ser.*, vol. 116, pp. 45–64, AGU, Washington, D. C.
- Dartevelle, S., G. G. J. Ernst, J. Stix, and A. Bernard (2002), Origin of the Mount Pinatubo climactic eruption cloud: Implications for volcanic hazards and atmospheric impacts, *Geology*, *30*, 663–666.
- DeFoor, T. E., E. Robinson, and S. Ryan (1992), Early lidar observations of the June 1991 Pinatubo eruption plume at Mauna Loa Observatory, Hawaii, *Geophys. Res. Lett.*, *19*, 187–190.
- Deshler, T., D. J. Hofmann, B. J. Johnson, and W. R. Rozier (1992), Balloonborne measurements of the Pinatubo aerosol size distribution and volatility at Laramie, Wyoming during the summer of 1991, *Geophys. Res. Lett.*, *19*, 199–202.
- Gerlach, T. M., H. R. Westrich, and R. B. Symonds (1996), Preeruption vapor in magma of the climactic Mount Pinatubo eruption: Source of the giant stratospheric sulfur dioxide cloud, in *Fire and Mud: Eruptions and Lahars of Mount Pinatubo, Philippines*, edited by C. G. Newhall and R. S. Punongbayan, pp. 415–433, Philippine Inst. of Volcanol. and Seismol., Quezon City.
- Gu, Y., W. I. Rose, and G. Bluth (2003), Retrieval of mass and sizes of particles in sandstorms using two MODIS IR bands: A case study of April 7, 2001 sandstorm in China, *Geophys. Res. Lett.*, *30*(15), 1805, doi:10.1029/2003GL017405.
- Guo, S., W. I. Rose, G. J. S. Bluth, C. Textor, and H.-F. Graf (2000), ATHAM model simulation of 15 June 1991 Pinatubo volcanic plume, *Eos Trans. AGU*, *80*(48), Fall Meet. Suppl., Abstract V62C-10.
- Guo, S., G. J. S. Bluth, W. I. Rose, I. M. Watson, and A. J. Prata (2004), Re-evaluation of SO<sub>2</sub> release of the 15 June 1991 Pinatubo eruption using ultraviolet and infrared satellite sensors, *Geochem. Geophys. Geosyst.*, *5*, Q04001, doi:10.1029/2003GC000654.
- Herzog, M., H.-F. Graf, C. Textor, and J. M. Oberhuber (1998), The effect of phase changes of water on the development of volcanic plumes, *J. Volcanol. Geotherm. Res.*, *87*, 55–74.
- Holasek, R. E., S. Self, and A. W. Woods (1996), Satellite observations and interpretation of the 1991 Mount Pinatubo eruption plumes, *J. Geophys. Res.*, *101*, 27,635–27,655.
- Jaeger, H. (1992), The Pinatubo eruption cloud observed by lidar at Garmisch-Partenkirchen, *Geophys. Res. Lett.*, *19*, 191–194.
- Kinne, S., O. B. Toon, and M. J. Prather (1992), Buffering of stratospheric circulation by changing amounts of tropical ozone: A Pinatubo case study, *Geophys. Res. Lett.*, *19*, 1927–1930.
- Kou, L., D. Labrie, and P. Chylek (1993), Refractive indices of water and ice in the 0.65 to 2.5 micron range, *Appl. Opt.*, *32*, 3531–3540.
- Krotkov, N. A., O. Torres, C. Seftor, A. J. Krueger, W. Rose, A. Kostinski, G. Bluth, D. Schneider, and S. J. Schaefer (1999), Comparison of TOMS and AVHRR volcanic ash retrievals from the August 1992 eruption of Mt. Spurr, *Geophys. Res. Lett.*, *26*, 455–458.
- Long, C. S., and L. L. Stowe (1994), Using the NOAA/AVHRR to study stratospheric aerosol optical thickness following the Mt. Pinatubo eruption, *Geophys. Res. Lett.*, *21*, 2215–2218.
- Mayberry, G. C., W. I. Rose, and G. J. S. Bluth (2002), Dynamics of volcanic and meteorological clouds produced on 26 December (Boxing Day) 1997 at Soufrière Hills Volcano, Montserrat, in *The eruption of Soufrière Hills Volcano, Montserrat, From 1995 to 1999*, edited by T. H. Druitt and B. P. Kokelaar, *Mem. Geol. Soc. London*, *21*, 539–555.
- McCormick, A. P., L. W. Thomason, and C. R. Trepte (1995), Atmospheric effects of Mt. Pinatubo eruption, *Nature*, *373*, 399–404.
- McPeters, R. D., et al. (1998), Nimbus-7 Total Ozone Mapping Spectrometer (TOMS) Data Product User's Guide, *NASA 1998-20,6895*, Goddard Space Flight Center, Greenbelt, Md.
- McPherson, R. D., K. H. Bergman, R. E. Kistler, G. E. Rasch, and D. S. Gordon (1979), The NMC operational global data assimilation system, *Mon. Weather Rev.*, *107*, 1445–1461.
- Neal, C. A., R. G. McGimsey, C. A. Gardner, M. L. Harbin, and C. J. Nye (1994), Tephra-fall from the 1992 eruptions of Crater Peak, Mount Spurr Volcano, AK: A preliminary report on distribution, stratigraphy and composition, *U.S. Geol. Surv. Bull.*, *2139*.

- Pollack, J. B., O. B. Toon, and B. N. Khare (1973), Optical properties of some terrestrial rocks and glasses, *Icarus*, *19*, 372–389.
- Prata, A. J. (1989a), Observation of volcanic ash clouds in 10–12 (m window using AVHRR/2 data, *Int. J. Remote Sens.*, *10*, 751–761.
- Prata, A. J. (1989b), Infrared radiative transfer calculations for volcanic ash clouds, *Geophys. Res. Lett.*, *16*(11), 1293–1296.
- Prata, A. J., W. I. Rose, S. Self, and D. M. O'Brien (2003), Global, long-term sulphur dioxide measurements from TOVS data: A new tool for studying explosive volcanism and climate, in *Volcanism and the Earth's Atmosphere*, *Geophys. Monogr. Ser.*, vol. 139, edited by A. Robock and C. Oppenheimer, pp 75–92, AGU, Washington, D. C.
- Read, W. G., L. Froidevaux, and J. W. Waters (1993), Microwave limb sounder measurement of stratospheric SO<sub>2</sub> from the Mt. Pinatubo volcano, *Geophys. Res. Lett.*, *20*, 1299–1302.
- Riley, C., W. Rose, and G. Bluth (2003), Quantitative shape measurements of distal volcanic ash, *J. Geophys. Res.*, *108*(B10), 2504, doi:10.1029/2001JB000818.
- Robock, A. (2002), The climate aftermath, *Science*, *295*, 1242–1243.
- Rose, W. I., D. J. Delene, D. J. Schneider, G. J. S. Bluth, A. J. Krueger, I. Sprod, C. McKee, H. L. Davies, and G. G. J. Ernst (1995), Ice in the 1994 Rabaul eruption cloud: Implications for volcano hazard and atmospheric effects, *Nature*, *375*, 477–479.
- Rose, W. I., G. J. S. Bluth, and G. G. J. Ernst (2000), Integrating retrievals of volcanic cloud characteristics from satellite remote sensors: A summary, *Philos. Trans. R. Soc. London, Ser. A*, *358*, 1585–1606.
- Rose, W. I., G. J. S. Bluth, D. J. Schneider, G. G. J. Ernst, C. M. Riley, L. J. Henderson, and R. G. McGimsey (2001), Observation of volcanic clouds in their first few days of atmospheric residence: The 1992 eruptions of Crater Peak, Mount Spurr volcano, Alaska, *J. Geol.*, *109*, 677–694.
- Rose, W. I., et al. (2003), The February-March 2000 eruption of Hekla, Iceland from a satellite perspective, in *Volcanism and the Earth's Atmosphere*, *Geophys. Monogr. Ser.*, vol. 139, edited by A. Robock and C. Oppenheimer, pp. 107–132, AGU, Washington, D. C.
- Russell, P. B., et al. (1996), Global to microscale evolution of the Pinatubo volcanic aerosol derived from diverse measurements and analyses, *J. Geophys. Res.*, *101*(D13), 18,745–18,763.
- Rutherford, M. J., and J. D. Devine (1996), Preeruption pressure-temperature conditions and volatiles in the 1991 Dacitic Magma of Mount Pinatubo, in *Fire and Mud: Eruptions and Lahars of Mount Pinatubo, Philippines*, edited by C. G. Newhall and R. S. Punongbayan, pp. 751–766, Philippine Inst. of Volcanol. and Seismol., Quezon City.
- Schneider, D. J., W. I. Rose, and L. Kelley (1995), Tracking of 1992 eruption clouds from Crater Peak vent of Mount Spurr volcano, Alaska, using AVHRR, in *The 1992 Eruptions of Crater Peak Vent, Mount Spurr Volcano, Alaska*, edited by T. E. C. Keith, *U.S. Geol. Surv. Bull.*, *2139*, 27–36.
- Schneider, D. J., W. I. Rose, L. R. Coke, G. J. S. Bluth, I. Sprod, and A. J. Krueger (1999), The first four days of volcano/atmosphere interaction following a stratospheric eruption as observed with TOMS and AVHRR, *J. Geophys. Res.*, *104*, 1037–1050.
- Schoeberl, M. R., L. R. Lait, P. A. Newman, and J. E. Rosenfield (1992), The structure of the polar vortex, *J. Geophys. Res.*, *97*, 7859–7882.
- Schoeberl, M. R., S. D. Doiron, L. R. Lait, P. A. Newman, and A. J. Krueger (1993), A simulation of the Cerro Hudson SO<sub>2</sub> cloud, *J. Geophys. Res.*, *98*, 2949–2955.
- Scott, W. E., R. P. Hoblitt, R. C. Torres, S. Self, M. M. L. Martinez, and T. Nillos (1996), Pyroclastic flows of the June 15, 1991 climactic eruption of Mount, Pinatubo, in *Fire and Mud: Eruptions and Lahars of Mount Pinatubo, Philippines*, edited by C. G. Newhall and R. S. Punongbayan, pp. 545–570, Philippine Inst. of Volcanol. and Seismol., Quezon City.
- Seftor, C. J., N. C. Hsu, J. R. Herman, P. K. Bhartia, O. Torres, W. I. Rose, D. J. Schneider, and N. Krotkov (1997), Detection of volcanic ash clouds from Nimbus 7/total ozone mapping spectrometer, *J. Geophys. Res.*, *102*, 16,749–16,759.
- Self, S., J.-X. Zhao, R. E. Holasek, R. C. Torres, and A. J. King (1996), The atmospheric impact of the 1991 Mount Pinatubo eruption, in *Fire and Mud: Eruptions and Lahars of Mount Pinatubo, Philippines*, edited by C. G. Newhall and R. S. Punongbayan, pp. 1089–1115, Philippine Inst. of Volcanol. and Seismol., Quezon City.
- Shannon, J. (1997), Three dimensional evolution of volcanic gas and ash clouds from Crater Peak, Mt. Spurr, M.S. thesis, Mich. Technol. Univ., Houghton.
- Solomon, S., R. W. Sanders, R. R. Garcia, and J. G. Keys (1993), Increased chlorine dioxide over Antarctica caused by volcanic aerosols from Mount Pinatubo, *Nature*, *363*, 245–248.
- Sparks, R. S. J., M. I. Bursik, S. N. Carey, J. S. Gilbert, L. Glaze, H. Sigurdsson, and A. W. Woods (1997), *Volcanic Plumes*, John Wiley, New York.
- Textor, C. (1999), Numerical simulation of scavenging processes in explosive volcanic eruption clouds, Ph.D. thesis, Max-Planck Inst. for Meteorol, Hamburg, Germany.
- Turco, R. P., O. B. Toon, R. C. Whitten, P. Hamill, and R. G. Keesee (1983), The 1980 eruption of Mount St. Helens: Physical and chemical processes in the stratospheric clouds, *J. Geophys. Res.*, *88*, 5299–5319.
- Wallace, J. M., and P. V. Hobbs (1997), *Atmospheric Science: An Introductory Survey*, Academic, San Diego, Calif.
- Watson, I. M., W. I. Rose, V. J. Realmuto, and G. J. S. Bluth (2003), Forward modeling of volcanic aerosols transmissions at different latitudes: Quantifying the effects of varying tropospheric water vapor on ash detection, *Eos Trans. AGU*, *84*(46), Fall Meet. Suppl., Abstract V12E-05.
- Wen, S., and W. I. Rose (1994), Retrieval of particle sizes and masses in volcanic clouds using AVHRR band 4 and band 5, *J. Geophys. Res.*, *99*, 5421–5431.
- Wiesner, M. G., A. Wetzel, S. G. Catane, E. L. Listanco, and H. T. Mirabueno (2004), Grain size, areal thickness distribution and controls on sedimentation of the 1991 Mount Pina-



- tubo tephra layer in the South China Sea, *Bull. Volcanol.*, *66*, 226–242, doi:10.1007/s00445-003-0306-x.
- Wolfe, E. W., and R. P. Hoblitt (1996), Overview of the eruptions, in *Fire and Mud: Eruptions and Lahars of Mount Pinatubo, Philippines*, edited by C. G. Newhall and R. S. Punongbayan, pp. 415–433, Philippine Inst. of Volcanol. and Seismol., Quezon City.
- Yamanouchi, T., K. Suzuki, and S. Kawaguchi (1987), Detection of clouds in Antarctica from infrared multispectral data of AVHRR, *J. Meteorol. Soc.*, *65*, 949–961.
- Yu, T., and W. I. Rose (2000), Retrieval of sulfate and silicate ash masses in young (1 to 4 days) eruption clouds using multiband infrared HIRS/2 data, in *Remote Sensing of Active Volcanism, Geophys. Monogr. Ser.*, vol. 116, edited by P. Mougini-Mark, J. Crisp, and J. Fink, pp. 87–100, AGU, Washington, D. C.
- Yu, T., W. Rose, and A. Prata (2002), Atmospheric correction for satellite-based volcanic ash mapping and retrievals using “split window” IR data from GOES and AVHRR, *J. Geophys. Res.*, *107*(D16), 4311, doi:10.1029/2001JD000706.